# A major endogenous glycosidase mediating quercetin uptake in *Bombyx mori*

Ryusei Waizumi*, Chikara Hirayama, Shuichiro Tomita, Tetsuya Iizuka, Seigou Kuwazaki, Akiya Jouraku, Takuya Tsubota, Kakeru Yokoi, Kimiko Yamamoto, Hideki Sezutsu

Institute of Agrobiological Sciences, National Agriculture and Food Research Organization (NARO), 1-2 Owashi, Tsukuba, Ibaraki 305-8634, Japan

*Correspondence:
Ryusei Waizumi
waizumir957@affrc.go.jp

## Abstract

Quercetin is a common plant flavonoid that is involved in herbivore–plant interactions. Mulberry silkworms (domestic silkworm, *Bombyx mori*, and wild silkworm, *Bombyx mandarina*) uptake quercetin from mulberry leaves and accumulate the metabolites in the cocoon, thereby improving its protective properties. Here we identified and characterized a glycosidase, named LPH-like quercetin glycoside hydrolase 1 (LQGH1), that initiates quercetin metabolism in the domestic silkworm. LQGH1 is expressed in the midgut where it mediates quercetin uptake by deglycosylating the three most common quercetin glycosides present in mulberry leaf: rutin, quercetin-3-*O*-malonyl-glucoside, quercetin-3-*O*-glucoside. Despite being located in an unequal crossing-over hotspot, *LQGH1* is conserved in some species in clade Macroheterocera, including the wild silkworm, indicating the adaptive significance of quercetin uptake. *LQGH1* is important also in breeding: defective mutations of *LQGH1*, which result in discoloration of the cocoon and increased silk yield, are homozygously conserved in 27 of the 32 Japanese white-cocoon domestic silkworm strains and 12 of the 30 Chinese ones we investigated.

## Introduction

Quercetin (3,3',4',5,7-pentahydroxyflavone) is a flavonoid abundantly found in a wide variety of plants [1]. Previous studies have found oviposition and feeding stimulant activity of quercetin glycosides on lepidopteran, orthopteran and coleopteran insects [2,3,4,5,6]. These suggest that quercetin is widely ingested by insects. Quercetin ingestion by insects is likely not merely a consequence of the identification and feeding on host plants; it may have adaptive significance. In the common blue butterfly (*Polyommatus icarus*), which sequesters quercetin-3-*O*-galactoside in its wings, flavonoid content is high in the female insects than in the males and positively correlated with female sex attraction [7,8,9]. The yellow pigment in the wings of a grasshopper (*Dissosteira carolina*), which possibly contributes to their camouflage in plants, is the result of sequestration of quercetin-3-*O*-glucoside (isoquercitrin, Q3G) [10]. Although these studies strongly emphasize the significance of quercetin in herbivore–plant interactions, the molecular mechanisms of quercetin metabolism in insects are poorly understood.

Mulberry silkworms (domestic silkworm, *Bombyx mori*, and wild silkworm, *Bombyx mandarina*) accumulate various compounds, including quercetin glucosides, kaempferol glucosides, and carotenoids, in their silk glands and colored cocoons (S1 Fig) [11,12,13]. Quercetin glucosides stored in the body and in the cocoon are reported to have antioxidant, ultraviolet-protective, and antibacterial properties [14,15,16]. Quercetin is found in the leaves of the mulberry tree (*Morus alba*), the sole food source of the mulberry silkworm, as a series of glycosides formed by glycosylation at the 3-*O* position. The three most common quercetin glycosides in mulberry are quercetin-3-*O*-rutinoside (rutin), quercetin-

3-*O*-malonyl-glucoside (Q3MG) and Q3G, which account for 71%–80% of the total flavonol content in the leaves [17].

The color of the cocoon of the domestic silkworm has been diversified through breeding, which indicates that the kinds and amounts of flavonoids that accumulate in the cocoons differ between strains [11,12]. Particularly, cocoons containing high flavonoid concentrations express a yellow-green color and are known as “green cocoons”. Because accumulation in the cocoon is the end step of flavonoid metabolism, forward-genetic analysis focused on cocoon flavonoid content can reveal the genes involved in each step of flavonoid metabolism. Indeed, several loci associated with flavonoid metabolism have already been identified through this approach: the *Green b* locus, which encodes a uridine 5’-diphospho-glucosyltransferase with a rare enzymic activity glycosylating the 5-*O* position of quercetin [14], and the *New Green Cocoon* (*Gn*) locus, which encodes clustered sugar transporters presumed to import quercetin glucosides from the hemolymph to the silk gland [18]. However, these findings explain only a part of the process from quercetin uptake to the final accumulation of its metabolites in the cocoon. Elucidating the steps of flavonoid metabolism in the silkworm can provide valuable insights into the understanding of herbivore–plant interactions.

Here, we performed a quantitative trait locus (QTL) analysis focused on cocoon flavonoid content in the domestic silkworm. We identified a novel locus, *Green d* (*Gd*), that is associated with cocoon flavonoid content. Within the locus, we identified a glycosidase gene, *LPH-like quercetin glycoside hydrolase 1* (*LQGH1*), that mediates quercetin uptake into the midgut cells by deglycosylating mulberry leaf-derived quercetin glycosides.

Genetic dissections of the novel gene revealed the contribution of the gene to improvement of the cocoon in the commercial context through breeding.

## Results

### QTL analysis identified a novel locus associated with flavonoid content in cocoon

To identify genes involved in quercetin metabolism by means of a forward-genetics approach, we prepared a green-cocoon strain (p50; alias: Daizo) and a white-cocoon strain (J01; alias: Nichi01). The two strains exhibited a distinct difference in cocoon color and flavonoid content (Fig 1A and 1B). A gradated range of cocoon colors in their F2 intercrossing offspring implied that the genetic differences between the two strains associated with flavonoid content were composite (Fig 1C). Therefore, we conducted a QTL analysis, which allows for simultaneous identification of multiple genetic loci involved in a phenotype of interest. The flavonoid content of the cocoons of the F2 population were scored by an absorbance-based method according to a previous report [19]. The QTL analysis was performed by using the phenotypic data of 102 individuals and 1038 genetic markers obtained from double-digest restriction-associated DNA sequencing data [20] (S1 Table). From the composite interval mapping, we identified three significant QTLs for cocoon flavonoid content on chromosomes 15, 20, and 27 (Fig 1C). Previous linkage studies have suggested a locus, named *Green c* (*Gc*) and associated with the yellow-green color of cocoons, at an unknown position on chromosome 15 [21,22]. The QTL on chromosome 27 was presumed to correspond to *Gn* [18]. Since no green cocoon-associated locus on chromosome 20 has yet been reported, we named that locus *Green d* (*Gd*). The contribution of the *Gd* locus to cocoon flavonoid content was the second largest of the three QTLs, with a percentage of phenotypic variation explained

by each QTL (PVE) value of 24.57% (Fig 1C, S2 Table). The 95% Bayes credible interval of the *Gd* locus was 7,980,189–10,504,065 bp. The nearest marker to *Gd* was located at 10,265,033 bp, with a logarithm of odds (LOD) score of 19.99. The PVE values of the QTLs on chromosomes 15 and 27 were 7.04% and 56.05%, respectively. Significant additive effects were detected between the QTLs on chromosomes 15 and 27, and between those on chromosomes 20 and 27, and the PVEs were 1.93% and 5.47%, respectively (S2 Table).

**_Gd_ locus contains a glycosidase cluster**

Using the genome assembly and gene models of p50T [23], we found on the *Gd* locus a cluster of nine genes encoding glycoside hydrolases (*KWMTBOMO12222–25*, *KWMTBOMO12227*, *KWMTBOMO12229*, *KWMTBOMO12230*, *KWMTBOMO12233*, and *KWMTBOMO12236*) (Fig 1D). In mammals, deglycosylation of quercetin glucosides by lactase/phlorizin hydrolase (LPH), a member of beta-glucosidase family 1, is a critical step in quercetin metabolism. LPH is expressed in intestinal epithelial cells and is anchored on the brush border membrane where it hydrolyzes flavonoid glycosides [24,25,26,27]. The resulting free quercetin aglycon is then passively absorbed into the intestinal cells due to its increased lipophilicity. We hypothesized that the glycosidases clustered within the *Gd* locus are involved in quercetin metabolism in the domestic silkworm, playing a role similar to that of LPH in mammals. To identify which of the *Gd* glycosidases act in the midgut, RNA-seq-based expression analysis was performed. Three of the candidate genes, *KWMTBOMO12222*, *KWMTBOMO12227*, and *KWMTBOMO12236*, were found to be strongly expressed in the midgut of p50T final instar larvae; the expression levels of these genes were significantly lower in the midgut

of strain J01 (Fig 1E). Further examination of the expression profiles of the three genes with high expression in the midgut revealed that *KWMTBOMO12227* and *KWMTBOMO12236* were expressed specifically in the midgut, whereas *KWMTBOMO12222* was expressed most in the malpighian tubule (S2 Fig). Thus, we identified *KWMTBOMO12222*, *KWMTBOMO12227*, and *KWMTBOMO12236* as candidate *Gd* genes which are involved in quercetin metabolism in the domestic silkworm .

**Functional analysis of the candidate *Gd* genes by CRISPR-Cas9**

To investigate the involvement of the candidate genes in the quercetin metabolism, we attempted to use a microinjection-mediated CRISPR-Cas9 system to establish p50T lineages in which the candidate genes had been knocked out. Although, we failed to establish knockout lineages for *KWMTBOMO12222* and *KWMTBOMO12236* due to the lethality of homozygous frame-shift mutations, we did manage to obtain two knockout lineages of *KWMTBOMO12227* with different types of frameshift mutations in exon 5. We designated the one with a 5-bp deletion as Δ*Gd1* and the other with a 2-bp deletion as Δ*Gd2* (Fig 2A). These mutations resulted in a premature stop codon at exon 5 and a shortened amino acid sequence length of KWMTBOMO12227 from 492 to 215 in Δ*Gd1* and to 216 in Δ*Gd2*. Further characterization revealed that compared to p50T the mutants produced discolored cocoons (Fig 2B). In addition, a reduction of fluorescence under ultraviolet irradiation, which is characteristic of the accumulation of the two major quercetin metabolites in silkworm (i.e., quercetin-5-*O*-glucoside and quercetin-5,4´-di-*O*-glucoside) [14,15,28], was observed in the midgut, hemolymph, and silk glands of the mutants (Fig 2C–2E), indicating reductions of flavonoid content in the mutant tissues.

Although knockout of *KWMTBOMO12227* reduced the total flavonoid content in the cocoon by less than half that in the original p50T strain, it was still much larger than the effect predicted for the *Gd* locus in the QTL analysis (Fig 2F and S2 Table). Similar reductions were found in the midgut, hemolymph, and middle and posterior silk gland. Because the flavonoid content in the cocoon differed largely between the insects reared with an artificial diet and those reared with fresh mulberry leaves (Fig 1B and Fig 2F), the flavonoid content reductions in the mutants were confirmed in an experiment using fresh mulberry leaves (S3 Fig). Together, these results indicate that knockout of *KWMTBOMO12227* results in malfunction of quercetin uptake into the midgut.

**Characterization of the protein sequence of the glycosidase encoded by *KWMTBOMO12227***

The CRISPR-Cas9-mediated knockout analysis strongly suggested that *KWMTBOMO12227* encodes a glycosidase which plays a crucial role in quercetin uptake in the domestic silkworm. *KWMTBOMO12227* consists of 11 exons, encoding a total of 492 amino acids. The accuracy of the modeled sequence was confirmed using the RNA-seq data obtained from final instar larvae of strain p50T (S1 Text). KWMTBOMO12227 was found to have an amino acid sequence similar to that of LPH, but phylogenetic inference suggested that KWMTBOMO12227 is not orthologous to LPH; it has evolved through gene duplication after the divergence of Pyraloidea and Macroheterocera (including Noctuoidea, Lasiocampoidea, and Bombycoidea) (S1 Text). Mature LPH harbors a transmembrane domain in the C-terminus region with which it is anchored to the brush border membrane [25]. A hydrophobic transmembrane domain was also

predicted in the first N-terminal 20 amino acid residues of KWMTBOMO12227 (S4 Fig), suggesting that the protein functions as a membrane-anchored glycosidase.

**LQGH1 mediates quercetin uptake by hydrolysis of quercetin glycosides**

Together, our knockout analysis and sequence characterization suggested that the glycosidase encoded by *KWMTBOMO12227* is anchored on the apical surface of epithelial cells and mediates the uptake of mulberry-derived quercetin by deglycosylation of quercetinglycosides in the midgut of the silkworm. However, some accumulation of flavonoids in the midgut was still observed in the knockout mutants (Fig 2F). This may be due to the diversity of quercetin glycosides in mulberry leaves and the substrate specificity of KWMTBOMO12227. To confirm whether *KWMTBOMO12227* is involved in deglycosylation of quercetin glycosides, we investigated the effect of knocking out the gene on the hydrolytic activity of midgut tissue on the three major quercetin glycosides in mulberry leaf: rutin, Q3MG, and Q3G (Fig 3A). To also examine the localization of KWMTBOMO12227, the midgut homogenate and the insoluble material fraction of that, including cell membranes, isolated from the homogenate by centrifugation, were used separately for the measurements.

The homogenate of the p50T midgut exhibited hydrolytic activity against all three types of quercetin glycoside (Fig 3B). However, the activities were decreased in the knockout mutants, indicating that KWMTBOMO12227 is involved in the hydrolysis of all three quercetin glycosides. Notably, *KWMTBOMO12227* knockout completely abolished the hydrolytic activity against rutin, indicating that KWMTBOMO12227 is the only glycosidase with hydrolytic activity against rutin. The hydrolytic activity of rutin was

196 stronger in the insoluble fraction than in the homogenate, supporting our assertion that
197 KWMTBOMO12227 is a membrane-anchored glycosidase. The reduction in the
198 hydrolytic activity of the other two glycosides, Q3MG and Q3G, was only partial,
199 suggesting that the silkworm has other glycosidases with hydrolytic activities against
200 those molecules (Fig 3B). The reduction in the hydrolytic activity of midgut homogenates
201 against Q3MG and Q3G by knocking out *KWMTBOMO12227* was 0.6 to 0.8-fold and
202 0.7 to 0.8-fold, respectively. The reduction in the hydrolytic activity of the insoluble
203 fraction against the two quercetin glycosides was 0.2 and 0.5-fold, respectively, which
204 were greater than those of the homogenate. These results suggest that
205 KWMTBOMO12227 is an important protein for the hydrolysis of quercetin glycosides
206 in the silkworm lumen. According to the characteristics of the protein sequence and
207 enzymatic activity of KWMTBOMO12227, we named the identified gene *LQGH1*.
208
209 In 1972, Fujimoto and Hayashiya reported that the domestic silkworm accumulates
210 flavonoids in its cocoon when reared on artificial diets containing isolated quercetin or
211 rutin but not when reared on mulberry leaves [29]. To investigate whether the uptake of
212 rutin-derived quercetin is dependent on deglycosylation by LQGH1, we reared insects on
213 semi-synthetic diets supplemented with rutin or quercetin but without mulberry leaf
214 powder and measured the flavonoid content in the cocoons. The p50T strain accumulated
215 flavonoids in its cocoon irrespective of diet (Fig 3C, 3D, and S3 Table). Although the
216 *LQGH1*-knockout mutants accumulated the same amount of flavonoids as did p50T when
217 reared on the quercetin diet, they accumulated only 6% of that accumulated by p50T when
218 reared on the rutin diet (Fig 3C and 3D). These results are consistent with the report by

Fujimoto and Hayashiya, and indicate that the uptake of quercetin from rutin is strongly dependent on deglycosylation by *LQGH1*.

**Defective structural mutations of *LQGH1* were broadly disseminated in white-cocoon domestic silkworm strains**

Although accumulation of carotenoids or flavonoids in the cocoon produces a variety of cocoon colors, it is white-cocoon strains that are the most popular in commercial use. Earlier in the present study, we found that defective mutation of *LQGH1* resulted in impaired quercetin absorption, which made the color of the cocoon closer to white (Fig 2B). Interestingly, the defective mutation of *LQGH1* did not impair the growth of the silkworm, but rather improved silk yield (S5 Fig). The implication here is that this beneficial mutation was selected for in the establishment of white-cocoon domestic silkworm strains.

To examine our hypothesis, we looked at the frequency and distribution of the defective mutation of *LQGH1* in a collection of *B. mori* strains. We first determined the details of the mutation introduced in J01. Previously, we reported a genome assembly and gene model for J01 [30]. A BLASTp search of our J01 gene model identified predicted gene *BMN13127* as the corresponding gene of *LQGH1* in J01. Comparing the genomic regions of *LQGH1* in the two strains, an insertion of 3997 bp was found in exon 5 of J01 *LQGH1*. Syntenic dot-plot analysis of the genomic sequences of exons 5, 6 and the intronic region between them (intron 5) of *LQGH1* of the two strains revealed that the inserted region contains the inverted sequence of intron 5 of p50T (Fig 4A). The inverted intron sequence was present at two sites within intron 5 of J01 *LQGH1*. In the genomic PCR amplifying

the region on exon 5, including the insertion, an amplified product from the J01 genomic DNA was approximately 4000-bp longer than that from the p50T genomic DNA (Fig 4B). Due to the insertion, the predicted protein sequence of J01 LQGH1 lacked 31 amino acid residues in the middle compared to that of p50T LQGH1 (S6 Fig). The deletion included two of nine residues with >99% conservation across 101 homologous proteins from five Macroheterocera species, and all of seven residues that harbored strongly similar physicochemical properties across the proteins (S7 Fig). These observations strongly suggest that the deletion is mainly responsible for the observed difference in flavonoid content in the cocoon.

Next, we examined the presence of the J01-type 4-kbp insertion in 67 Japanese and Chinese local strains by PCR using tested primers (S8 Fig and S4 Table). All five green-cocoon strains lacked the insertion. Of the 32 Japanese local white-cocoon strains, the insertion was absent in five, present in seven, and no amplification product was observed in 20. Of the 30 Chinese local white-cocoon strains, the insertion was absent in 15, present in three (p50T-type products were also observed in these strains), and no amplification product was observed in 11. The lack of an amplification product suggested strains with another dysfunctional mutation. To determine the mutation, we assembled the genomic sequence of one of the strains without an observed amplification product, Kosetsu, using the Illumina whole-genome sequencing data. By comparison against the genomic sequence of p50T, a 143.7-kbp deletion including *LQGH1* was found in the Kosetsu *Gd* locus (Fig 4C). When the region including the deletion was amplified by PCR using p50T, J01, and Kosetsu genomic DNA, an observable amplification product was synthesized only from the Kosetsu sample (Fig 4D). In addition, no observable amplification product

was synthesized from the Kosetsu sample by reverse-transcription PCR amplifying the full-length open reading frame of *LQGH1* using cDNA from the midgut of sixth-day final instar larvae of the three strains (Fig 4E). The J01-derived product was shorter in size and had a weaker signal compared to that from p50T. These results are consistent with the genetic differences of *Gd* among the three strains predicted from the assembled genomic sequences. Integrating the genotyping results using primer sets to identify this large deletion, we successfully genotyped the 62 strains. The five strains with no observable amplification product in the PCR have possibly undergone further genome sequence changes by unequal crossing-over after acquiring the Kosetsu-type large deletion (S8 Fig).

To summarize the genomic PCR analysis, three haplotypes of *LQGH1* were found in the population: p50T-type (P), J01-type (J, harboring a 4-kbp insertion in exon 5), and Kosetsu-type (K, harboring a large deletion eliminating *LQGH1*). The proportions of strains homozygous for the functional haplotype (P), heterozygous for the functional and a dysfunctional (J or K) haplotype, and homozygous for a dysfunctional haplotype were 3%, 13%, and 84%, respectively, in the Japanese local white-cocoon strains, and 23%, 37%, and 40%, respectively, in the Chinese local white-cocoon strains (Fig 4F).

## Discussion

### LQGH1 mediates quercetin uptake in *Bombyx mori*

Here, we identified LQGH1 as a glycosidase that initiates quercetin metabolism in the domestic silkworm. LQGH1 is expressed specifically in the midgut and is indicated to be localized on the apical surface of the epithelial cells with a transmembrane domain at the N-terminal (S2 and S4 Fig). Knockout of *LQGH1* reduced total flavonoid content in the

midgut, hemolymph, and silk glands, indicating that the gene is involved in quercetin uptake into the midgut (Fig 2C–2F). The hydrolytic activity of the midgut tissue on rutin, Q3MG, and Q3G was reduced in *LQGH1*-knockout mutants (Fig 3B), indicating that LQGH1 hydrolyses all three major quercetin glycosides present in mulberry leaf. The greater rutin hydrolytic activity in the midgut insoluble fraction than in the homogenate supported that LQGH1 is a membrane-anchored protein (Fig 3B). The amount of flavonoids contained in the cocoon of insects reared with a diet supplemented with rutin was greatly reduced in the absence of functional LQGH1 (Fig 3C and 3D), suggesting that deglycosylation of quercetin glycosides by LQGH1 is a critical step in quercetin uptake. However, the present functional analyses were limited to genetic analyses using genome editing. Further biochemical and/or immunological studies will be needed to clarify the enzymatic characteristics and biological role of LQGH1.

While revealing a major role for LQGH1 in quercetin uptake in the silkworm, this study also suggests the presence of LQGH1-independent quercetin glycoside digestion pathways. The accumulation of flavonoids in the cocoon and tissues was not completely lost in the *LQGH1*-knockout mutants (Fig 2F). In addition, the residual hydrolytic activity of the insoluble material fraction of the midgut on Q3MG and Q3G implies the presence of other glycosidases mediating quercetin uptake (Fig 3B). Although we were unable to successfully obtain lineages in which *KWMTBOMO12222* and *KWMTBOMO12236* were knocked out, their proteins are possibly the identities of these other glycosidases. In addition, the hydrolytic activity of Q3MG and Q3G in the *LQGH1*-knockout mutant was higher in the homogenate than in the insoluble material fraction (Fig 3B), implying that

digestion of quercetin glycosides also occurs in the midgut cells by unanchored glycosidases.

**Adaptive significance of quercetin uptake in mulberry silkworm is supported by the fact that LQGH1 has acquired and conserved rutin hydrolytic activity**

Our results show that LQGH1 mediates quercetin uptake in the domestic silkworm in a deglycosylation-dependent manner, similar to LPH in mammals. However, our data indicate that *LQGH1* is not an ortholog corresponding to mammalian *LPH*, rather it has evolved through gene duplications during Lepidoptera diversification and has acquired a peculiar function, rutin hydrolytic activity (Fig 3, S10 and S11 Figs, S1 Text). *In vitro*, LPH hydrolyses Q3MG and Q3G, but not rutin [24,26,31]. Rutin hydrolysis in mammals is dependent on the intestinal microbiota [32]. It also depends on the gut microbiota in the honey bee (*Apis mellifera*) [33]. Rutin glycosidases have previously been identified in bacteria, fungi, and plants [34,35,36], but to our knowledge, not in animals. Rutin is a common plant flavonoid, accounting for 14%–46% of flavonol glycosides in mulberry leaf [17]. The accumulation of flavonoids in the cocoon of *LQGH1*-knockout mutants reared on a rutin-containing diet was severely restricted, indicating the absence of rutin digestion pathways other than deglycosylation by LQGH1 (Fig 3C and 3D). Therefore, the acquisition of rutin hydrolytic activity should result in a considerable change in quercetin intake. In addition, the phylogenetic tree of the lepidopteran proteins indicated that frequent gene duplication events in the *Gd* glycosidase family have occurred (S11 Fig). In the inference of gene duplication events by Orthofinder [37], the number of events in the LQGH1-included group was the most frequent among 55 ortholog groups including 78 silkworm proteins annotated as glycosidases (S5 and S6 Table). While the genomic

instability of the *Gd* locus had possibly provided genetic materials to evolve *LQGH1* by gene duplication events, it can be inferred to have repeatedly exposed *LQGH1* to a crisis of loss by unequal crossing-over. However, *LQGH1* remained conserved until its defective mutation was selected in breeding. This emphasizes the significance of quercetin bioavailability brought about by *LQGH1*; our study supports that the suggested positive properties of quercetin glycosides, their antioxidant [15], ultraviolet light-protective [14], and antibacterial functions [16], improve the fitness of the wild silkworm in the natural environment. Although, it should be noted that excessive quercetin uptake is still toxic even for the domestic silkworm [38], meaning that the mulberry silkworms should have a mechanism to maintain appropriate levels of quercetin. The fluorescence in the posterior region of the midgut observed in the present study implied accumulation of quercetin glucosides with glycosylation at the 5-*O* position and the reloading of excessive quercetin glucosides from the hemolymph to excrete them into the midgut lumen (Fig 2C).

**_LQGH1_ loss contributed to cocoon improvement**

Through breeding, many strains of the domestic silkworm have been established that exhibit a wide variety of cocoon colors depending on their flavonoid and carotenoid content, but commercially white cocoons tend to be preferred in regions such as Japan and China, especially since the 20th century. In a previous study that conducted a worldwide genetic analysis of silkworm strains, 91 of the 121 strains examined were white-cocoon strains [39]. The defective mutation in *LQGH1*, which manifests as reduced cocoon color (Fig 2B), may have contributed to the establishment of these white-cocoon silkworm strains. Of the white-cocoon strains examined in the present study, the

362 proportion with homozygous defective haplotypes of *LQGH1* (haplotype J or K) was only
363 62% (Fig 4F, S8 Fig, and S4 Table). In 24% of the strains, a mixture of defective and
364 functional haplotypes (haplotype P) was present. These are not surprising results,
365 considering that not all white-cocoon strains harbor loss-of-function mutations of the
366 sugar transporters on the *Gn* locus, which is more effective than *Gd* with respect to cocoon
367 discoloration [18]. Even if visually determined as white, the actual color tone and
368 therefore the flavonoid content of the cocoon varies from strain to strain [40]. In addition
369 to *Gd*, *Gb*, and *Gn*, within each of which a gene involved in the quercetin metabolism has
370 been identified, several loci associated with cocoon greenness have been reported,
371 including *Gc* [21,22], *Green cocoon* (*Grc*), *Green egg shell* (*Gre*), and *Yellow fluorescent*
372 (*Yf*) [21]. "White cocoon" is presumed to be expressed by additive cocoon color
373 discoloration by a combination of loss-of-function haplotypes of these loci.
374
375 Although loss of *LQGH1* is not necessarily essential for cocoon whiteness, given the high
376 conservation rate of loss-of-function haplotypes and the fact that knockout of the gene
377 reduced the cocoon total flavonoid content by less than half (Fig 2F, Fig 4F), the gene
378 still makes an important contribution to cocoon discoloration in the domestic silkworm.
379 Interestingly, the knockout of *LQGH1* increased the cocoon weight (S5 Fig). Because
380 endoreduplication is an important step in silkworm silk gland development [41],
381 interference with the replication step by quercetin interaction with DNA may explain the
382 relationship between *LQGH1* and silk yield [42]. Although it will be difficult to confirm
383 this hypothesis because cocoon weight is a complex quantitative trait dependent on
384 silkworm physiology and behavior, elucidation of the relationship between quercetin and
385 silk yield may provide clues to further improve silkworm protein productivity.

386

387 **Materials and Methods**

388 **Insect materials**

389 All domestic silkworm strains used in the present study were maintained at the National
390 Agriculture and Food Research Organization (NARO, Japan). p50T, the strain used for
391 the functional analysis of *LQGH1*, is almost genetically identical to p50, because the
392 strain is a descendant strain of p50 that had undergone repeated passage using a single
393 pair to improve homozygosity for referential use. The silkworms were reared on a
394 commercial artificial diet (SilkMate PM; Nosan, Kanagawa, Japan) or fresh mulberry
395 leaves under a controlled environment (12-h light/dark photoperiod, 25°C). Insects reared
396 on fresh mulberry leaves were used for measurement of the flavonoid contents of the
397 cocoons of p50 and J01 (Fig 1A and 1B), the scoring for QTL analysis (Fig 1C), and
398 measurement of the flavonoid contents of the cocoons of p50T and *LQGH1*-knockout
399 mutants (S3 Fig). All individuals, except those from which genomic DNA and RNA-seq
400 data were derived, were female.

401

402 **Flavonoid content measurement**

403 Flavonoids in cocoons were extracted with MeOH–$H_2O$ (7:3, V/V) at 60ºC for 2 h, after
404 shredding the cocoons into 2–3-mm squares. The extraction was repeated twice for
405 thorough extraction. The flavonoid content in the solution was derived from the
406 absorption at 365 nm, which is highly correlated with flavonoid content ($r$ = 0.95) [19].
407 In the case of flavonoid content as an input for QTL analysis, the raw values of the
408 absorbance were used as relative phenotype scores. The tissues and organs for measuring
409 flavonoid content were sampled from sixth-day final instar larvae reared on the

commercial artificial diet, rinsed well with PBS buffer (pH 7.4) (Takara Bio, Shiga, Japan), and stored at −80ºC. Immediately after collection, to inhibit melanization, 0.5 M sodium dimethyldithiocarbamate (Fujifilm, Tokyo, Japan) was added to reach 0.5% by volume to the collected hemolymph. Quantification of flavonoid content in the samples was performed according to a previous report [15] with some modifications. In brief, 30 µL of sample was injected into an LC-10ADVP HPLC system equipped with an SPD-10AV photodiode array detector (both Shimadzu Co., Kyoto, Japan) and separated with a Sunfire C18 column (150 × 3.0 mm i.d.; Waters, Massachusetts, USA) at a flow rate of 1.0 mL/min. Spectrum analysis and flavonoid peak assignment were performed with the CLASS-VP HPLC software (Shimadzu Co.). Flavonoids were quantified using quercetin 5, 4´-di-*O*-glucoside as the reference compound.

**QTL analysis**

The intercross F2 population of p50T and J01 used in the present study were the same samples as those sequenced by double-digest restriction-associated DNA sequencing and used to generate linkage maps in our previous study [30]. The sequencing data of 102 female F2 individuals are available in the Sequence Read Archive under the BioProject accession number PRJDB13956. The raw values of absorbance, indicating the relative cocoon flavonoid content for each individual, are summarized in S1 Table. The method for genotyping, marker selection, and construction of linkage maps is described in detail in our previous report [30]. Briefly, OneMap v2.8.2 [43] was used to construct linkage maps with an LOD score of 3, with the genotype of the F2 population output from the script “ref_map.pl” in STACKS v1.48 [44] as the input. The p50T genome assembly was used as the reference for read mapping [23]. The linkage map used consisted of 1038

makers, covered a total genetic length of 945.36 cM, and had an average marker density of 0.936 cM. QTL analysis was performed using the R/qtl v1.46.2 package [45], with the relative flavonoid content scores in the cocoons and the genetic position of markers linked to the physical position on the p50T genomic sequence as inputs. Using the "calc.genoprob" function in R/qtl, the probabilities of the true underlying genotypes were calculated with a step size of 1 cM and an assumed genotyping error rate of 0.05. QTL detection was performed by composite interval mapping using the function "cim" with the following parameters: method = "hk", n.marcovar = 3, window = 10. The LOD significance threshold for detecting QTL was calculated by a permutation test of 1000 trials. Approximate Bayesian 95% credible intervals were calculated using the function "bayesint". The positions of the nearest markers outside of the boundaries of a confidence interval were defined as the ends of the interval. PVEs and additive effects of the three significant QTLs were estimated using the function "fitqtl" with the parameter: formula = y ~ Q1 + Q2 + Q3 + Q1 * Q2 * Q3.

**Gene editing**

CHOPCHOP v3 was used to identify target sites [46]. Each 20-nucleotide guide sequence was unique on the p50T genomic sequence [23]. The construction of DNA templates for the synthesis of single-guide RNA (sgRNA) was performed according to a previous report [47]. Briefly, the DNA template, which included the T7 promoter, sgRNA target with PAM motif, and tracrRNA-complemental sequence, was synthesized by template-free PCR. A MEGAshortscript T7 Transcription Kit (Thermo Fisher Scientific, Waltham, Massachusetts, U.S.A.) was used for *in vitro* sgRNA transcription and template DNA digestion. A Guide-it IVT RNA Clean-Up Kit (Takara Bio) was used to clean up the

458 sgRNA solution. Alt-RS.p. HiFi Cas9 Nuclease V3 solution (Integrated DNA
459 Technologies, Coralville, Iowa, U.S.A.) and the sgRNA were mixed with distilled water
460 to final concentrations of 500 ng/μL and 50 ng/μL, respectively. The Cas9 nuclease and
461 sgRNA mixed solution was incubated for 1 h at room temperature to allow the
462 ribonucleoprotein to form. The ribonucleoprotein solution was microinjected into non-
463 diapause eggs of the p50T strain within 8 h after oviposition, in accordance with a
464 previous report [48]. Non-diapause treatment was performed by incubating the eggs under
465 17°C short-day conditions (12-h light/dark photoperiod) until hatching. Adult moths of
466 G0 individuals (injected generation) were crossed with wild-type moths. High-resolution
467 melting (HRM) analysis using genomic DNA extracted from molt shells of the G1
468 generations in cocoons identified individuals harboring identical heterozygous mutant
469 haplotypes. PCR for HRM analysis was performed by using a KAPA HRM Fast PCR Kit
470 (Roche, Basel, Switzerland) on a LightCycler 96 System (Roche) according to the
471 manufacturer's instruction. Genomic DNA extraction from molt shells was performed by
472 homogenizing the shells in a typical SDS-based lysis buffer followed by isopropanol
473 precipitation. By the same method, G2 individuals with a homozygous mutant haplotype
474 were identified and crossed, establishing the knockout lines. PCR products including the
475 target site were sequenced using a BigDye Terminator v3.1 Cycle Sequencing Kit and an
476 Applied Biosystems 3130xl Genetic Analyzer (Thermo Fisher Scientific) to confirm the
477 mutation. The primer sequences used are listed in S7 Table.
478
479 **Photographing of dissected samples**
480 Sixth-day fifth instar larvae reared on the artificial diet were used. Photographs were
481 collected with a DP74 camera (Olympus, Tokyo, Japan) attached to an SZX16

482 microscope (Olympus). Immediately after collection, to inhibit melanization, 0.5 M
483 sodium dimethyldithiocarbamate (Fujifilm) was added to reach 0.5% by volume to the
484 collected hemolymph. Silk glands and whole-body samples from which silk glands had
485 been removed were rinsed well with PBS buffer (pH 7.4) (Takara Bio) before imaging to
486 remove fluorescent hemolymph. A fluorescence light source U-HGLGPS (Olympus) and
487 ultraviolet light filter set (excitation: 330–385 nm, emission: 420 nm longpass) (Olympus)
488 were used for imaging under ultraviolet light irradiation. Because of the loss of resolution
489 and optical noise when the field of view was made large enough to fit the whole body,
490 the whole-body samples were photographed in segments and then the pictures were
491 combined. In the photographs shown in Fig 2, no post-editing of any kind, other than
492 cropping, was performed.
493
494 **Isoform identification and expressional analysis**
495 RNA-seq data from the midgut and other organs of third-day fifth instar larvae of p50T
496 and J01 were previously published by our research group [30,49]. The sequencing reads
497 were trimmed by fastp v0.20.0 [50] with the following parameters: -q 20 -n 5 -l 100. The
498 mapping of the reads to the p50T genome assembly and transcript isoform identification
499 were conducted using HISAT2 v2.1.0 [51] and SrtingTie2 v2.2.0 [52] with the default
500 parameters. Salmon v1.5.2 [53] was used to calculate transcripts per kilobase million
501 scores. The modeled transcript sequence of p50T was used as the reference [23].
502
503 **Phylogenetic analysis**
504 To collect protein sequences for constructing the phylogenetic tree of glycosidases of
505 mammals and insects (S10 Fig), the related proteins were collected by BLASTp search

using the predicted protein sequence of *KWMTBOMO12227* of the p50T strain gene model as the query sequence [23]. Genes with e-values less than 1E-50 were used for the analysis. The KEGG [54] BLAST search service (https://www.genome.jp/tools/blast/) was used for picking related proteins in *Rattus norvegicus*, *Drosophila melanogaster*, *Tribolium castaneum*, and *Apis mellifera*. The query and these sequences were aligned using Clustal Omega v1.2.4 [55]. Tree construction by the neighbor-joining method was performed using MEGA 11 [56]. The number of bootstrap trials was set to 100. The phylogenetic tree of lepidopteran orthologs of the *Gd* glycosidases was constructed by the maximum likelihood method using RAxML-NG v1.1 [57] with the following parameters: --bs-trees 100, --model LG+I+G4 (S11 Fig A). The best-fit phylogenetic analysis model was suggested using ModelTest-NG v0.1.7 [58]. Gene models of 12 lepidopteran insects available in InsectBase 2.0 [59] (http://v2.insect-genome.com/) were used (*Papilio Xuthus*, *Megathymus ursus*, *Lycaena phlaeas*, *Limenitis camilla*, *Chilo suppressalis*, *Biston betularia*, *Pheosia gnoma*, *Dendrolimus punctatus*, *Bombyx mori*, *Bombyx mandarina*, *Antheraea yamamai*, *Deilephila porcellus*); each of the models were predicted based on high-quality genome sequences using long-read sequencing, and their BUSCO [60] scores were all above 94%. Rat LPH (NCBI RefSeq accession: NP_446293) and the total of 90 protein sequences of the lepidopteran species determined by Orthofinder [37] v2.5.2 to belong to the same ortholog group as any of the nine *Gd* glycosidases were used in the analysis.

**Assay for hydrolytic activity of the midgut**

Midguts of fifth-day final instar larvae reared on the commercial artificial diet were collected, rinsed well with PBS buffer (pH 7.4) (Takara Bio), and immediately stored at

530 −80ºC. Three times the weight of 10 mM phosphate/1 mM PMSF buffer (pH 7.5) as the
531 samples was added and they were homogenized. Centrifugation at 20,000*g* for 20 min,
532 collection of the precipitate fraction, and washing with the buffer were repeated twice for
533 the homogenate sample to obtain an insoluble fraction containing cell membranes.
534 Hydrolysis was performed in a 20 mM phosphoric acid (pH 5.5) solution with quercetin
535 glycosides at a concentration of 2 mM for 4 h at 37ºC. The reaction was stopped by adding
536 three volumes (V/V) of methanol. Control incubations in which the substrates were
537 omitted were also run. After centrifugation at 20,000*g* for 10 min, the quercetin content
538 of the supernatant was quantified with the HPLC system as described in the section
539 "Flavonoid content measurement." Quercetin, rutin, and Q3G were obtained from
540 Extrasynthese (Lyon, France). Q3MG was obtained from Merck (Darmstadt, Germany).
541 Hydrolytic activity toward the quercetin glycosides is expressed as nanomoles of
542 quercetin produced per min per mg protein. The protein concentration in the enzyme
543 preparations was measured with a commercial assay kit (Coomassie Plus, Thermo Fisher
544 Scientific).
545
546 **Dietary administration of quercetin or rutin**
547 Silkworm larvae were reared on the commercial diet from hatching to the third ecdysis,
548 then the fourth instar larvae were fed with a diet containing 25% mulberry leaf powder
549 [61]. The newly molted fifth instar larvae were reared on semi-synthetic diets
550 supplemented with quercetin or rutin, which did not contain mulberry leaf powder (S3
551 Table). Flavonoids added to the diets were approximately equimolar (0.1 mmol/100-g dry
552 diet). Chlorogenic acid was added to the diets as a feeding stimulant. Soybean meal (Soya
553 flour FT; Nisshin OilliO Group,. Ltd., Tokyo, Japan) was washed twice with five volumes

554 of 90% (V/V) ethanol to remove deterrent substances and allowed to dry naturally before
555 use in the diets.
556
557 **Genomic comparison of the *Gd* locus**
558 Dot-plot analysis was performed using FlexiDot v1.06 [62] with the following
559 parameters: -p 1 -f 1 -A 2 -E 100. The illustrated exon-intron structure of J01 *LQGH1*
560 (*BMN13127*) was modified from the original model (Fig 4A); the incorrect prediction of
561 exon 1 was modified according to *KWMTBOMO12227*, and the J01 transcript sequence
562 was obtained by using the original RNA-seq data [30]. DNA extraction of the domestic
563 silkworm strain Kosetsu from the whole body of a male larva was performed by a typical
564 phenol-chloroform-based method. Whole genomic sequencing was performed using an
565 Illumina NovaSeq 6000 Sequencing System (Illumina Inc., San Diego, USA) via an
566 outsourcing service (Macrogen Japan Corp., Kyoto, Japan). The sequencing generated
567 50.4 Gb of paired-end reads with a length of 151 bp. Genome assembly of the Kosetsu
568 strain was performed using MaSuRCA v4.0.9 [63] with pseudomolecule sequences of
569 chromosomes 15, 20, and 27 of p50T [23], on which the QTLs are present, as the
570 assembly reference. The parameter defining 20 times genomic size "JF_SIZE" was set to
571 9,000,000,000. The input genomic sequencing data of the Kosetsu strain was trimmed by
572 fastp v0.20.0 [46] with the following parameters before assembly: -q 20 -n 5 -l 100.
573
574 **PCR-based genotyping**
575 The genomic DNA of each strain was extracted from 10 pairs of silk glands of final instar
576 larvae by a typical phenol-chloroform-based method. The final concentration of genomic
577 DNA was conditioned to 0.5 ng/μL. KOD One PCR Master Mix -Blue- (Toyobo, Osaka,

578 Japan) was used for PCR. The times and temperatures of preincubation, denaturation,
579 annealing, and extension were set to 30 s at 95°C, 10 s at 98°C, 10 s at 60°C, and 45 s at
580 68°C, respectively, for 32 cycles. The primer sequences used are listed in S7 Table.
581
582 **Reverse-transcription PCR**
583 Total RNA was extracted from the midgut of sixth-day final instar larvae using ISOGEN
584 (Nippon Gene, Tokyo, Japan) according to the manufacturer's instructions.
585 Contaminating DNA in the RNA solution was digested using RNase-Free DNase Set
586 (Qiagen, Hilden, Germany). The isolated RNA was purified using an RNeasy Kit
587 (Qiagen). Equal volumes of RNA solutions from five individuals, adjusted to the same
588 concentration, were mixed to obtain a single bulk sample. Reverse transcription was
589 performed using ReverTra Ace qPCR RT Master Mix (Toyobo) according to the
590 manufacturer's instruction, and the final concentration of the RNA was conditioned to 10
591 ng/μL. RT-PCR was performed using KAPA HiFi HotStart ReadyMix (Roche) under
592 conditions that resulted in 1% of the concentration of the original cDNA solution. The
593 times and temperatures of preincubation, denaturation, annealing, and extension were set
594 to 180 s at 95°C, 5 s at 98°C, 10 s at 60°C, and 60 s at 72°C, respectively, for 28 cycles.
595 The primer sequences used are listed in S7 Table.
596
597 **Detecting gene duplication events**
598 Detecting gene duplication events in lepidopteran *Gd* glysosidases was performed using
599 Orthofinder v2.5.2 [37] together with the ortholog-group inference for the phylogenetic
600 analysis. The glycosidase gene was identified in the domestic silkworm by referencing
601 the annotation file of silkworm protein using InterProScan [64] within KAIKObase [65]

(https://kaikobase.dna.affrc.go.jp/index.html). Proteins annotated as "Glycoside hydrolase superfamily (IPR017853)" or with the functional annotation "hydrolase activity, acting on glycosyl bonds (GO:0016798)" were considered to be proteins annotated as glycosidases.

**Other informatic tools**

Handling sequences: Seqkit v2.2.0 [66]; statistical calculations: R v4.0.3 (R Foundation for Statistical Computing, Vienna, Austria); illustrating graphs: ggplot2 v3.4.1 [67] and ggpubr v0.6.0 (https://CRAN.R-project.org/package=ggpubr); prediction of hydrophobic transmembrane domains: SOSUI v1.11 [68]; illustrating structural formulae: Ketcher v2.8.0 (https://github.com/epam/ketcher); genomic browsing: Integrative Genomics Viewer v2.12.3 [69]; phylogenetic tree editing: Interactive Tree Of Life v5 [70].

**Supplementary information**

Supplementary materials are available at Figshare. doi: 10.6084/m9.figshare.23553015

**Data availability**

The raw genomic sequencing data of the Kosetsu strain are available in the Sequence Read Archive under the BioProject accession number PRJDB15366.

**Acknowledgements**

We thank Ms. Mayuko Sakatoh for her technical assistance; Sae Furuhashi, Toshihiko Misawa, Kaoru Nakamura, Keita Hiruma, Koji Hashimoto, and Eiji Okada for their support in the silkworm rearing; Hiroki Sakai for giving instruction on the CRISPR-Cas9

system construction; and Nobuto Yamada for giving instruction on the microinjection. The computation was partly performed using the supercomputer of the Agriculture, Forestry and Fisheries Research Information Technology Center of the Japanese Ministry of Agriculture, Forestry and Fisheries.

## Author contributions

RW: Conceptualization, Data Curation, Formal Analysis, Investigation, Visualization, Writing – original draft preparation, Writing – review & editing; CH: Conceptualization, Investigation, Writing – review & editing; ST: Resources, Writing – review & editing, Supervision; TI: Conceptualization, Funding Acquisition, Investigation, Project Administration, Resources; SK: Investigation; AJ: Investigation, Writing – review & editing; TT: Resources, Writing – review & editing; KYo: Resources; KYa: Supervision; HS: Funding Acquisition, Supervision

## Funding

This work was financially supported by grants from the Japanese Ministry of Agriculture, Forestry and Fisheries, and JSPS KAKENHI Grant Numbers 21H03831 to K.Y. and H.S.. The funders had no role in study design, data collection and analysis, decision to publish, or preparation of the manuscript.

## Competing interests

The authors declare no competing interests.

## References

650 1. Cao J, Chen W, Zhang Y, Zhang Y, Zhao X. Content of Selected Flavonoids in 100
651 Edible Vegetables and Fruits. FSTR. 2010;16: 395–402. doi:10.3136/fstr.16.395
652 2. Bernays EA, Howard JJ, Champagne D, Estesen BJ. Rutin: a phagostimulant for the
653 polyphagous acridid Schistocerca americana. Entomologia Experimentalis et Applicata.
654 1991;60: 19–28. doi:10.1111/j.1570-7458.1991.tb01518.x
655 3. Hamamura Y, Hayashiya K, Naito K-I, Matsuura K, Nishida J. Food Selection By
656 Silkworm Larvae. Nature. 1962;194: 754–755. doi:10.1038/194754a0
657 4. Haribal M, Renwick JAA. Oviposition stimulants for the monarch butterfly: Flavonol
658 glycosides from Asclepias curassavica. Phytochemistry. 1996;41: 139–144.
659 doi:10.1016/0031-9422(95)00511-0
660 5. Matsuda K. Feeding Stimulation of Flavonoids for Various Leaf Beetles (Coleoptera :
661 Chrysomelidae). Applied Entomology and Zoology. 1978;13: 228–230.
662 doi:10.1303/aez.13.228
663 6. Tebayashi S, Matsuyama S, Suzuki T, Kuwahara Y, Nemoto T, Fujii K.
664 Quercimeritrin: The Third Oviposition Stimulant of the Azuki Bean Weevil from the Host
665 Azuki Bean. J Pestic Sci. 1995;20: 299–305. doi:10.1584/jpestics.20.299
666 7. Burghardt F, Knüttel H, Becker M, Fiedler K. Flavonoid wing pigments increase
667 attractiveness of female common blue (Polyommatus icarus) butterflies to mate-searching
668 males. Naturwissenschaften. 2000;87: 304–307. doi:10.1007/s001140050726
669 8. Burghardt F, Proksch P, Fiedler K. Flavonoid sequestration by the common blue
670 butterfly Polyommatus icarus: quantitative intraspecific variation in relation to larval
671 hostplant, sex and body size. Biochemical Systematics and Ecology. 2001;29: 875–889.
672 doi:10.1016/S0305-1978(01)00036-9

673 9. Schittko U, Burghardt F, Fiedler K, Wray V, Proksch P. Sequestration and distribution
674 of flavonoids in the common blue butterfly Polyommatus icarus reared on Trifolium
675 repens. Phytochemistry. 1999;51: 609–614. doi:10.1016/S0031-9422(98)00746-8
676 10. Hopkins TL, Ahmad SA. Flavonoid wing pigments in grasshoppers. Experientia.
677 1991;47: 1089–1091. doi:10.1007/BF01923349
678 11. Fujimoto N, Hayashiya K. Studies on the pigments of cocoon. (VIII) On the
679 classification of the silkworm races and its geographical distribution from the viewpoint
680 of the rate of cocoon pigment contents. Journal of Insect Biotechnology and Sericology.
681 1961;30: 83–88. doi:10.11416/kontyushigen1930.30.83
682 12. Hirayama C, Kosegawa E, Tamura Y, Nakamura M. Analysis of flavonoids in the
683 cocoon layer of the silkworm regional races by LC-MS. SANSHI-KONCHU BIOTEC.
684 2009;78: 57–63. doi:10.11416/konchubiotec.78.1_57
685 13. Sakudoh T, Sezutsu H, Nakashima T, Kobayashi I, Fujimoto H, Uchino K, et al.
686 Carotenoid silk coloration is controlled by a carotenoid-binding protein, a product of the
687 Yellow blood gene. Proceedings of the National Academy of Sciences. 2007;104: 8941–
688 8946. doi:10.1073/pnas.0702860104
689 14. Daimon T, Hirayama C, Kanai M, Ruike Y, Meng Y, Kosegawa E, et al. The
690 silkworm Green b locus encodes a quercetin 5-O-glucosyltransferase that produces green
691 cocoons with UV-shielding properties. Proceedings of the National Academy of Sciences.
692 2010;107: 11471–11476. doi:10.1073/pnas.1000479107
693 15. Hirayama C, Ono H, Tamura Y, Konno K, Nakamura M. Regioselective formation of
694 quercetin 5-O-glucoside from orally administered quercetin in the silkworm, Bombyx
695 mori. Phytochemistry. 2008;69: 1141–1149. doi:10.1016/j.phytochem.2007.11.009

16. Kurioka A, Ishizaka H, Yamazaki M, Endo M. Antibacterial activity of cocoon shells. J Silk Sci Tech Jpn. 1999;8: 57–60. doi:10.11417/silk.8.57

17. Sugiyama M, Katsube T, Koyama A, Itamura H. Varietal Differences in the Flavonol Content of Mulberry (Morus spp.) Leaves and Genetic Analysis of Quercetin 3-(6-Malonylglucoside) for Component Breeding. J Agric Food Chem. 2013;61: 9140–9147. doi:10.1021/jf403136w

18. Lu Y, Luo J, An E, Lu B, Wei Y, Chen X, et al. Deciphering the Genetic Basis of Silkworm Cocoon Colors Provides New Insights into Biological Coloration and Phenotypic Diversification. Molecular Biology and Evolution. 2023;40: msad017. doi:10.1093/molbev/msad017

19. Hirayama C, Okada E. Simple Spectrophotometric Analysis of Flavonoids from the Cocoon Shell of the Silkworm, Bombyx mori. J Silk Sci Tech Jpn. 2014;22: 65–70. doi:10.11417/silk.22.65

20. Peterson BK, Weber JN, Kay EH, Fisher HS, Hoekstra HE. Double Digest RADseq: An Inexpensive Method for De Novo SNP Discovery and Genotyping in Model and Non-Model Species. PLOS ONE. 2012;7: e37135. doi:10.1371/journal.pone.0037135

21. Fujii H, Banno Y, Doira H, Kihara H, Kawaguchi Y. Genetical Stocks and Mutations of Bombyx mori: Important Genetic Resoueces. 2nd ed. 1998.

22. Fujimoto N. On the physiological functions of the genes concerning the formation and the translocation of the pigments of green cocoon in silkworm larvae. The Journal of Sericultural Science of Japan. 1963;32: 338–342. doi:10.11416/kontyushigen1930.32.338

718 23. Kawamoto M, Jouraku A, Toyoda A, Yokoi K, Minakuchi Y, Katsuma S, et al. High-
719 quality genome assembly of the silkworm, Bombyx mori. Insect Biochemistry and
720 Molecular Biology. 2019;107: 53–62. doi:10.1016/j.ibmb.2019.02.002
721 24. Day AJ, Cañada FJ, Díaz JC, Kroon PA, Mclauchlan R, Faulds CB, et al. Dietary
722 flavonoid and isoflavone glycosides are hydrolysed by the lactase site of lactase phlorizin
723 hydrolase. FEBS Letters. 2000;468: 166–170. doi:10.1016/S0014-5793(00)01211-4
724 25. Mantei N, Villa M, Enzler T, Wacker H, Boll W, James P, et al. Complete primary
725 structure of human and rabbit lactase-phlorizin hydrolase: implications for biosynthesis,
726 membrane anchoring and evolution of the enzyme. The EMBO Journal. 1988;7: 2705–
727 2713. doi:10.1002/j.1460-2075.1988.tb03124.x
728 2**6**. Németh K, Plumb GW, Berrin J-G, Juge N, Jacob R, Naim HY, et al. Deglycosylation
729 by small intestinal epithelial cell β-glucosidases is a critical step in the absorption and
730 metabolism of dietary flavonoid glycosides in humans. Eur J Nutr. 2003;42: 29–42.
731 doi:10.1007/s00394-003-0397-3
732 27. Wacker H, Keller P, Falchetto R, Legler G, Semenza G. Location of the two catalytic
733 sites in intestinal lactase-phlorizin hydrolase. Comparison with sucrase-isomaltase and
734 with other glycosidases, the membrane anchor of lactase-phlorizin hydrolase. Journal of
735 Biological Chemistry. 1992;267: 18744–18752. doi:10.1016/S0021-9258(19)37024-3
736 28. Tamura Y, Nakajima K, Nagayasu K, Takabayashi C. Flavonoid 5-glucosides from
737 the cocoon shell of the silkworm, Bombyx mori. Phytochemistry. 2002;59: 275–278.
738 doi:10.1016/S0031-9422(01)00477-0
739 29. Fujimoto N, Hayashiya K. Studies on the pigments of cocoon. (IX) The precursor of
740 the pigments of green cocoon in the silkworm, Bombyx mori. Journal of Insect

741 Biotechnology and Sericology. 1972;41: 383–386.
742 doi:10.11416/kontyushigen1930.41.383
743 30. Waizumi R, Tsubota T, Jouraku A, Kuwazaki S, Yokoi K, Iizuka T, et al. Highly
744 accurate genome assembly of an improved high-yielding silkworm strain, Nichi01. G3
745 Genes|Genomes|Genetics. 2023;13. doi:10.1093/g3journal/jkad044
746 31. Ioku K, Pongpiriyadacha Y, Konishi Y, Takei Y, Nakatani N, Terao J. beta-
747 Glucosidase activity in the rat small intestine toward quercetin monoglucosides. Biosci
748 Biotechnol Biochem. 1998;62: 1428–1431. doi:10.1271/bbb.62.1428
749 32. Riva A, Kolimár D, Spittler A, Wisgrill L, Herbold CW, Abrankó L, et al. Conversion
750 of Rutin, a Prevalent Dietary Flavonol, by the Human Gut Microbiota. Frontiers in
751 Microbiology. 2020;11. Available:
752 https://www.frontiersin.org/articles/10.3389/fmicb.2020.585428
753 33. Kešnerová L, Mars RAT, Ellegaard KM, Troilo M, Sauer U, Engel P. Disentangling
754 metabolic functions of bacteria in the honey bee gut. PLOS Biology. 2017;15: e2003467.
755 doi:10.1371/journal.pbio.2003467
756 34. Beekwilder J, Marcozzi D, Vecchi S, de Vos R, Janssen P, Francke C, et al.
757 Characterization of Rhamnosidases from Lactobacillus plantarum and Lactobacillus
758 acidophilus. Applied and Environmental Microbiology. 2009;75: 3447–3454.
759 doi:10.1128/AEM.02675-08
760 35. Pachl P, Kapešová J, Brynda J, Biedermannová L, Pelantová H, Bojarová P, et al.
761 Rutinosidase from Aspergillus niger: crystal structure and insight into the enzymatic
762 activity. The FEBS Journal. 2020;287: 3315–3327. doi:10.1111/febs.15208

763 36. Sun Y, Cui X, Wang Z. Characterization of a rutin-hydrolyzing enzyme with β-
764 glucosidase activity from tartary buckwheat (Fagopyrum tartaricum) seeds. Food Sci
765 Technol. 2022;42: e42822. doi:10.1590/fst.42822
766 37. Emms DM, Kelly S. OrthoFinder: phylogenetic orthology inference for comparative
767 genomics. Genome Biology. 2019;20: 238. doi:10.1186/s13059-019-1832-y
768 38. Shi G, Kang Z, Ren F, Zhou Y, Guo P. Effects of Quercetin on the Growth and
769 Expression of Immune-Pathway-Related Genes in Silkworm (Lepidoptera: Bombycidae).
770 Bendena B, editor. Journal of Insect Science. 2020;20: 23. doi:10.1093/jisesa/ieaa124
771 39. Xiang H, Liu X, Li M, Zhu Y, Wang L, Cui Y, et al. The evolutionary road from wild
772 moth to domestic silkworm. Nat Ecol Evol. 2018;2: 1268–1279. doi:10.1038/s41559-
773 018-0593-4
774 40. Hirayama C, Kosegawa E. Identification of fluorescence in white cocoon shells of the
775 silkworm based on three-dimensional fluorescence spectroscopy. SANSHI-KONCHU
776 BIOTEC. 2021;90: 189–194. doi:10.11416/konchubiotec.90.3_189
777 41. Perdrix-Gillot S. DNA synthesis and endomitoses in the giant nuclci of the silkgland
778 of Bombyx mori. Biochimie. 1979;61: 171–204. doi:10.1016/S0300-9084(79)80066-8
779 42. Srivastava S, Somasagara RR, Hegde M, Nishana M, Tadi SK, Srivastava M, et al.
780 Quercetin, a Natural Flavonoid Interacts with DNA, Arrests Cell Cycle and Causes
781 Tumor Regression by Activating Mitochondrial Pathway of Apoptosis. Sci Rep. 2016;6:
782 24049. doi:10.1038/srep24049
783 43. Margarido GRA, Souza AP, Garcia A a. F. OneMap: software for genetic mapping in
784 outcrossing species. Hereditas. 2007;144: 78–79. doi:10.1111/j.2007.0018-0661.02000.x

785 44. Catchen JM, Amores A, Hohenlohe P, Cresko W, Postlethwait JH. Stacks: Building
786 and Genotyping Loci De Novo From Short-Read Sequences. G3
787 Genes|Genomes|Genetics. 2011;1: 171–182. doi:10.1534/g3.111.000240
788 45. Broman KW, Wu H, Sen Ś, Churchill GA. R/qtl: QTL mapping in experimental
789 crosses. Bioinformatics. 2003;19: 889–890. doi:10.1093/bioinformatics/btg112
790 46. Labun K, Montague TG, Krause M, Torres Cleuren YN, Tjeldnes H, Valen E.
791 CHOPCHOP v3: expanding the CRISPR web toolbox beyond genome editing. Nucleic
792 Acids Research. 2019;47: W171–W174. doi:10.1093/nar/gkz365
793 47. Kistler KE, Vosshall LB, Matthews BJ. Genome Engineering with CRISPR-Cas9 in
794 the Mosquito Aedes aegypti. Cell Reports. 2015;11: 51–60.
795 doi:10.1016/j.celrep.2015.03.009
796 48. Tamura T, Thibert C, Royer C, Kanda T, Abraham E, Kamba M, et al. Germline
797 transformation of the silkworm Bombyx mori L. using a piggyBac transposon-derived
798 vector. Nat Biotechnol. 2000;18: 81–84. doi:10.1038/71978
799 49. Yokoi K, Tsubota T, Jouraku A, Sezutsu H, Bono H. Reference Transcriptome Data
800 in Silkworm Bombyx mori. Insects. 2021;12: 519. doi:10.3390/insects12060519
801 50. Chen S, Zhou Y, Chen Y, Gu J. fastp: an ultra-fast all-in-one FASTQ preprocessor.
802 Bioinformatics. 2018;34: i884–i890. doi:10.1093/bioinformatics/bty560
803 51. Kim D, Paggi JM, Park C, Bennett C, Salzberg SL. Graph-based genome alignment
804 and genotyping with HISAT2 and HISAT-genotype. Nat Biotechnol. 2019;37: 907–915.
805 doi:10.1038/s41587-019-0201-4
806 52. Kovaka S, Zimin AV, Pertea GM, Razaghi R, Salzberg SL, Pertea M. Transcriptome
807 assembly from long-read RNA-seq alignments with StringTie2. Genome Biology.
808 2019;20: 278. doi:10.1186/s13059-019-1910-1

809 53. Patro R, Duggal G, Love MI, Irizarry RA, Kingsford C. Salmon provides fast and
810 bias-aware quantification of transcript expression. Nat Methods. 2017;14: 417–419.
811 doi:10.1038/nmeth.4197
812 54. Ogata H, Goto S, Sato K, Fujibuchi W, Bono H, Kanehisa M. KEGG: Kyoto
813 Encyclopedia of Genes and Genomes. Nucleic Acids Research. 1999;27: 29–34.
814 doi:10.1093/nar/27.1.29
815 55. Sievers F, Wilm A, Dineen D, Gibson TJ, Karplus K, Li W, et al. Fast, scalable
816 generation of high-quality protein multiple sequence alignments using Clustal Omega.
817 Molecular Systems Biology. 2011;7: 539. doi:10.1038/msb.2011.75
818 56. Tamura K, Stecher G, Kumar S. MEGA11: Molecular Evolutionary Genetics
819 Analysis Version 11. Molecular Biology and Evolution. 2021;38: 3022–3027.
820 doi:10.1093/molbev/msab120
821 57. Kozlov AM, Darriba D, Flouri T, Morel B, Stamatakis A. RAxML-NG: a fast,
822 scalable and user-friendly tool for maximum likelihood phylogenetic inference. Wren J,
823 editor. Bioinformatics. 2019;35: 4453–4455. doi:10.1093/bioinformatics/btz305
824 58. Darriba D, Posada D, Kozlov AM, Stamatakis A, Morel B, Flouri T. ModelTest-NG:
825 A New and Scalable Tool for the Selection of DNA and Protein Evolutionary Models.
826 Crandall K, editor. Molecular Biology and Evolution. 2020;37: 291–294.
827 doi:10.1093/molbev/msz189
828 59. Mei Y, Jing D, Tang S, Chen X, Chen H, Duanmu H, et al. InsectBase 2.0: a
829 comprehensive gene resource for insects. Nucleic Acids Research. 2022;50: D1040–
830 D1045. doi:10.1093/nar/gkab1090
831 60. Manni M, Berkeley MR, Seppey M, Zdobnov EM. BUSCO: Assessing Genomic Data
832 Quality and Beyond. Current Protocols. 2021;1: e323. doi:10.1002/cpz1.323

833 61. Hirayama C, Konno K, Shinbo H. The pathway of ammonia assimilation in the
834 silkworm, Bombyx mori. Journal of Insect Physiology. 1997;43: 959–964.
835 doi:10.1016/S0022-1910(97)00045-0
836 62. Seibt KM, Schmidt T, Heitkam T. FlexiDot: highly customizable, ambiguity-aware
837 dotplots for visual sequence analyses. Hancock J, editor. Bioinformatics. 2018;34: 3575–
838 3577. doi:10.1093/bioinformatics/bty395
839 63. Zimin AV, Marçais G, Puiu D, Roberts M, Salzberg SL, Yorke JA. The MaSuRCA
840 genome assembler. Bioinformatics. 2013;29: 2669–2677.
841 doi:10.1093/bioinformatics/btt476
842 64. Zdobnov EM, Apweiler R. InterProScan – an integration platform for the signature-
843 recognition methods in InterPro. Bioinformatics. 2001;17: 847–848.
844 doi:10.1093/bioinformatics/17.9.847
845 65. Yang C, Yokoi K, Yamamoto K, Jouraku A. An update of KAIKObase, the silkworm
846 genome database. Database. 2021;2021: baaa099. doi:10.1093/database/baaa099
847 66. Shen W, Le S, Li Y, Hu F. SeqKit: A Cross-Platform and Ultrafast Toolkit for
848 FASTA/Q File Manipulation. PLOS ONE. 2016;11: e0163962.
849 doi:10.1371/journal.pone.0163962
850 67. Wickham H. ggplot2: Elegant Graphics for Data Analysis. New York, NY: Springer;
851 2009. doi:10.1007/978-0-387-98141-3
852 68. Hirokawa T, Boon-Chieng S, Mitaku S. SOSUI: classification and secondary
853 structure prediction system for membrane proteins. Bioinformatics. 1998;14: 378–379.
854 doi:10.1093/bioinformatics/14.4.378
855 69. Robinson JT, Thorvaldsdóttir H, Winckler W, Guttman M, Lander ES, Getz G, et al.
856 Integrative genomics viewer. Nat Biotechnol. 2011;29: 24–26. doi:10.1038/nbt.1754

857 70. Letunic I, Bork P. Interactive Tree Of Life (iTOL) v5: an online tool for phylogenetic
858 tree display and annotation. Nucleic Acids Research. 2021;49: W293–W296.
859 doi:10.1093/nar/gkab301
860 71. Kawahara AY, Plotkin D, Espeland M, Meusemann K, Toussaint EFA, Donath A, et
861 al. Phylogenomics reveals the evolutionary timing and pattern of butterflies and moths.
862 Proceedings of the National Academy of Sciences. 2019;116: 22657–22663.
863 doi:10.1073/pnas.1907847116

864

865 **Figure legends**

866 Fig 1. Quantitive trait loci (QTLs) associated with cocoon flavonoid content.

867 (A) Photographs of representative cocoons of the p50 and J01 silkworm strains. Bar = 30

868 mm. (B) Flavonoid content of the cocoon of p50 and J01. Data are means ± SD. (C) QTL

869 analysis for cocoon flavonoid content. The horizontal dotted line indicates the threshold

870 of the permutation test (trials = 1000). Phenotype scores on the frequency distribution are

871 relative to a maximum measurement of 10. LOD, logarithm of odds; PVE, percentage of

872 phenotypic variation explained by each QTL. According to a previous study [21], the *Gc*

873 locus is located on chromosome 15, but the detailed genetic or physical position is

874 unknown. Therefore, it cannot be concluded that the QTL peak on chromosome 15

875 identified here corresponds to the *Gc* locus. (D) Modelled genes present within the *Gd*

876 locus of the p50T genome assembly. The genes annotated as encoding a glycosyl

877 hydrolase are highlighted in black; their IDs are *KWMTBOMO12222*,

878 *KWMTBOMO12223*, *KWMTBOMO12224*, *KWMTBOMO12225*, *KWMTBOMO12227*,

879 *KWMTBOMO12229*, *KWMTBOMO12230*, *KWMTBOMO12233*, and

880 *KWMTBOMO12236* from the upstream side. (E) Expression of the candidate *Gd* genes

881 in the midgut of third-day final instar male larvae. Data are means ± SD. TPM, transcripts

882 per million.

883

884 Fig 2. Reduction of flavonoid content in *KWMTBOMO12227*-knockout mutants.

885 (A) Disrupted target sequences in *KWMTBOMO12227*. (B)–(E) Cocoons (B), midguts

886 (C), hemolymph (D), and silk glands (E) of the p50T strain and the *KWMTBOMO12227*

887 mutants. Organs and tissues were taken from sixth-day final instar female larvae. Bars =

888 10 mm. (F) Total flavonoid content of cocoons, organs, and tissues of the p50T strain and

889 the *KWMTBOMO12227* mutant lineages. Data are means ± SD. All insects were reared
890 on a commercial artificial diet. SG, silk gland.
891
892 Fig 3. Hydrolytic activity of KWMTBOMO12227 on the three major quercetin
893 glycosides in mulberry leaf.
894 (A) Structural formulae of quercetin and the three major quercetin glycosides present in
895 mulberry leaf. (B) Hydrolytic activity of the midgut on the quercetin glycosides. Data are
896 means ± SD. The values above the graph are *p*-values calculated by a two-tailed Student's
897 *t*-test. The samples used were all fifth-day final instar female larvae reared on a
898 commercial artificial diet. (C) Photograph of representative cocoons of the p50T strain
899 and the mutants reared on semi-synthetic diets containing quercetin or rutin. Bar = 20
900 mm. (D) Total flavonoid content in the cocoon of the p50T strain and the mutants reared
901 on semi-synthetic diets containing quercetin or rutin. Data are means ± SD.
902
903 Fig 4. Conserved structural mutations of *LQGH1* in the domestic silkworm population.
904 (A) Dot-plot analysis of the genomic region of exons 5, 6 and the intronic region between
905 them (intron 5) of *LQGH1* from the p50T and J01 strains. (B) PCR identifying the J01-
906 type insertion. The amplified region is indicated by the colored area in (A). The primer
907 set amplifying the genomic region from exons 1 and 2 of *KWMTBOMO14639* (*rp49*) was
908 used as the control (predicted fragment length = 1548 bp). (C) Schematic illustration
909 comparing the *Gd* loci of the p50T and Kosetsu strains. Black boxes indicate the modeled
910 genes. (D) PCR identifying the Kosetsu-type large deletion. The amplified region is
911 indicated by the colored area in (C). (E) RT-PCR of the *LQGH1* full-length open reading
912 frame by using cDNA libraries constructed using the midguts of sixth-day final instar

913 larvae. The primer set targeting exons 1 and 2 of *KWMTBOMO14639* (*rp49*) was used as
914 the control (predicted fragment length = 213 bp). (F) Distribution of the haplotypes of
915 *LQGH1* in Japanese and Chinese local silkworm strains. P/P, only the p50T genotype was
916 detected; P/J/K, p50T, J01, and Kosetsu genotypes were detected; J/J, only the J01
917 genotype was detected; J/K, both J01 and Kosetsu genotypes were detected; K/K, only
918 the Kosetsu genotype was detected; U, unknown, nothing detected. Grayscale colors
919 indicate pairs of loss-of-function haplotypes.

920

## Description of supplementary materials

S1 Fig. Photographs of representative cocoons of the wild silkworm, *Bombyx mandarina*. A fresh mulberry leaf and cocoons of the wild silkworm in a bright field (left) and those irradiated with ultraviolet light A in a dark field (right). The cocoons under ultraviolet irradiation exhibit fluorescence that is characteristic of quercetin-5-*O*-glucoside and quercetin-5,4´-di-*O*-glucoside, the major quercetin metabolites in the silkworm tissues and cocoon [14,15,28]. The cocoons were collected in June 2023 at Tsukuba, Ibaraki, Japan. Bar = 10 mm.

S2 Fig. Expression profile of the candidate genes within the *Gd* locus in third-day final instar larva of the p50T strain.
All organs and tissues, except for ovaries, were taken from male larvae. Data are means ± SD. SG, silk gland; TPM, transcripts per million.

S3 Fig. Total flavonoid content in the cocoons of the p50T strain and the *KWMTBOMO12227*-knockout lineages reared on fresh mulberry leaves.
Data are means ± SD.

S4 Fig. Prediction of a transmembrane domain in the amino acid sequence of KWMTBOMO12227 by using the SOSUI tool.

S5 Fig. Weight of pupa and cocoon of p50T and the knockout mutants of *LQGH1*.
(A) Weight of the pupa. (B) Weight of the cocoon. The values above the graph are *p*-values calculated by Student's *t*-test. The crosses inside the boxes indicate the means.

945

946 S6 Fig. Alignment of the amino acid sequences of LQGH1 from the p50T and J01 strains.
947 Amino acid sequences were aligned using Clustal Omega.

948

949 S7 Fig. Alignment of LQGH1-like proteins in Macroheterocera species.
950 (A) Whole alignment of 101 LQGH1-like proteins in Macroheterocera species. Amino
951 acid residues identical to LQGH1 at positions with >99% conservation are highlighted by
952 blue. The 100 homologous proteins were collected by a BLASTp search using the amino
953 acid sequence of LQGH1 from each protein sequence data of *Bombyx mori* (KWMT),
954 *Antheraea yamamai* (Ayam), *Deilephila porcellus* (Dpor), *Dendrolimus punctatus*
955 (Dpun) and *Pheosia gnoma* (Pgno) with a cutoff criterion e-value of <1E-100. The
956 sequence data of *B. mori* were obtained from KAIKObase
957 (https://kaikobase.dna.affrc.go.jp/index.html) and those of *A. yamamai*, *D. porcellus* and
958 *P. gnoma* were obtained from InsectBase 2.0 (http://v2.insect-genome.com/). The
959 sequences were aligned using Clustal Omega. (B) Magnified view of J01-type deletion
960 region of the alignment. Descriptions of the consensus symbols indicating the
961 conservation level of amino acid residues are available at the Clustal Omega FAQ
962 (https://www.ebi.ac.uk/seqdb/confluence/display/THD/Help+-+Clustal+Omega+FAQ).
963 In brief, ':' indicates residues that harbor a strongly similar physicochemical property to
964 that in LQGH1, and '.' indicates residues that harbor a weakly similar physicochemical
965 property to that in LQGH1.

966

967 S8 Fig. Genotyping of the *Gd* locus of Japanese or Chinese local white-cocoon strains.

968 Haplotypes of the strains were determined by PCR genotyping. P/P, only the p50T
969 genotype was detected; P/J/K, all p50T, J01, and Kosetsu genotypes were detected; J/J,
970 only the J01 genotype was detected; J/K, both the J01 and Kosetsu genotypes were
971 detected; K/K, only the Kosetsu genotype was detected; U, unknown, nothing detected.
972 The primer set amplifying the genomic region from exons 1 to 2 of *KWMTBOMO14639*
973 (*rp49*) was used as the control (predicted fragment length = 1548 bp). The grey dotted
974 lines are straight lines connecting band markers of known size (M) that were applied at
975 both ends of the samples. These lines represent sizes of 4000, 200, 500, and 1500 bp,
976 from top to bottom. “JL” and “CL” stand for “Japanese local” and “Chinese local”,
977 respectively. The colors indicate the color of the cocoon.
978
979 S9 Fig. RNA-seq read alignment to the genomic sequence of *KWMTBOMO12227*.
980 (A) Mapping result of the midgut-derived RNA-seq reads and *KWMTBOMO12227*
981 transcript isoforms visualized with Integrative Genomics Viewer. Coverages on each
982 exon and splice junctions of three replicates are illustrated on tracks R1–3. (B) Coverage
983 mean of each base of exon 10 and the 15-bp extension region. Data are means ± SD.
984
985 S10 Fig. Phylogenetic tree of insect and rat proteins related to KWMTBOMO12227.
986 Values on the nodes represent the bootstrap score (trials = 100). Unreliable nodes with
987 bootstrap values under 50 are shown as multi-branching nodes. Arabidopsis thioglucoside
988 glucohydrolase 1 (TGG1) was used as the outgroup.
989
990 S11 Fig. Phylogenetic tree of *Gd* glycosidase orthologs in Lepidoptera.

(A) The phylogenetic tree was constructed by the maximum likelihood method. Values on the nodes represent the bootstrap score (trials = 100). Unreliable nodes with bootstrap values under 50 are shown as multi-branching nodes. Rat LPH was used as the outgroup. Red branches represent clades including the silkworm *Gd* glycosidases. Genes of the domestic silkworm are marked in bold. (B) Species tree of Lepidoptera with reference to the report by Kawahara et al. [71]. Red circles indicates species harboring an LQGH1 ortholog.

S1 Table. Information of the F2 individuals, parents, and phenotypic score used for the QTL analysis.

S2 Table. QTLs associated with flavonoid content in cocoon.

S3 Table. Composition of the semi-synthetic diets supplemented with quercetin or rutin.

*Amount added per 100 g dry diet: $K_2HPO_4$, 2.25 g; $CaCO_3$, 1.0g; KCl, 0.50 g; $MgSO_4$, 0.3 g; $FePO_4 \cdot 4H_2O$, 0.10g; $ZnCl_2$, 0.01 g.

** This mixture includes cellulose powder (61.76 g/100 g). Amount added per 100 g dry diet: biotin, 0.2 mg; choline-HCl, 150 mg; folic acid, 0.2 mg; inositol, 200 mg; nicotinic acid, 10 mg, Ca-pantothenate, 15 mg; pyridoxine-HCl, 3 mg; riboflavin, 2 mg; thiamine-HCl, 2 mg.

*** Amount added per 100 g dry diet: propionic acid, 0.75 mL; chloramphenicol, 15 mg.

S4 Table. Summary of the Japanese and Chinese local silkworm strains examined.

S5 Table. Orthogroups of the 12 species of Lepidoptera and numbers of detected gene duplication events.

S6 Table. Domestic silkworm glycosidases.

S7 Table. Primers used in the experiments.

S1 Text. Determination and phylogenetic characterization of the amino acid sequence of KWMTBOMO12227.

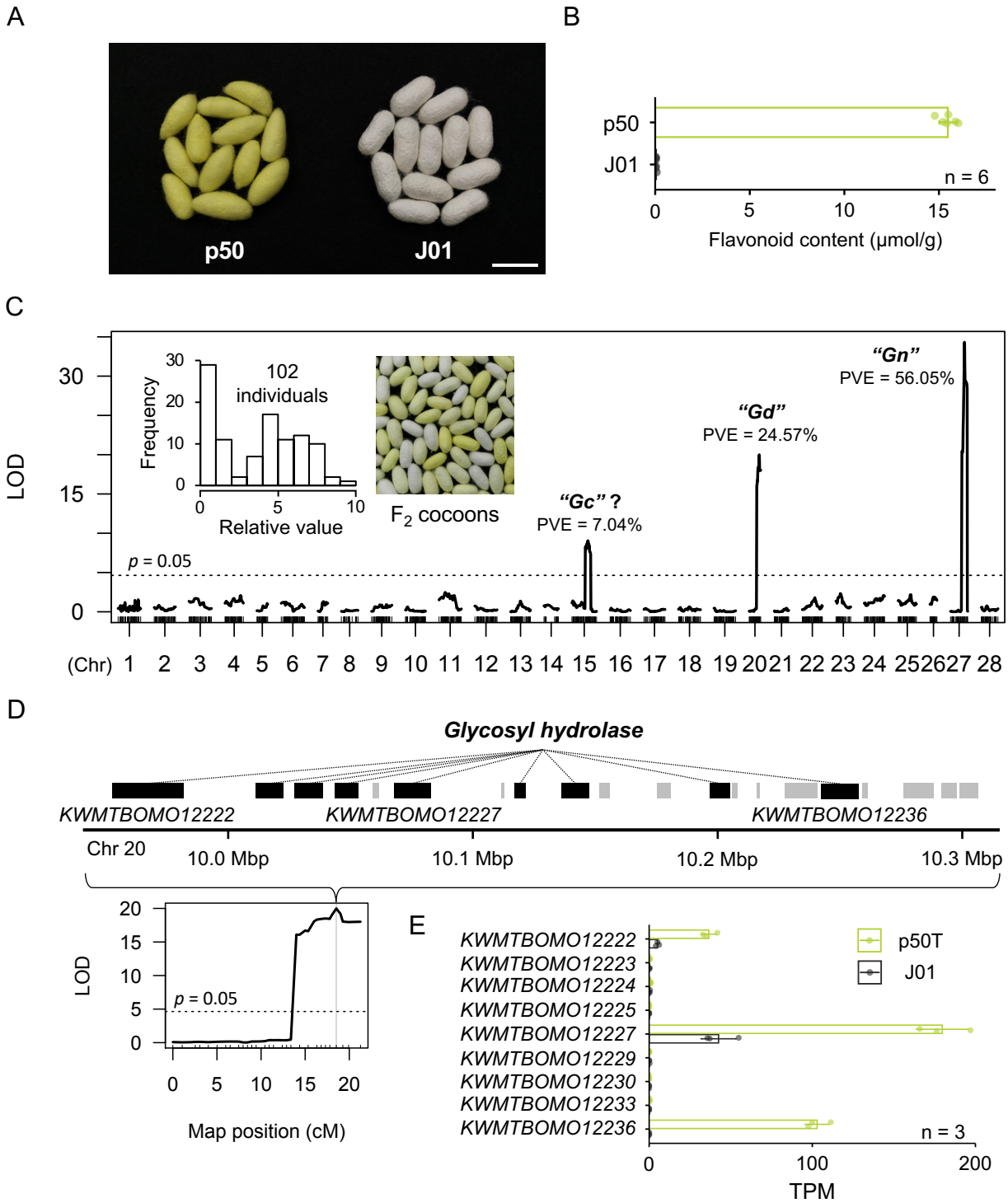


Fig 1. Quantitive trait loci (QTLs) associated with cocoon flavonoid content.

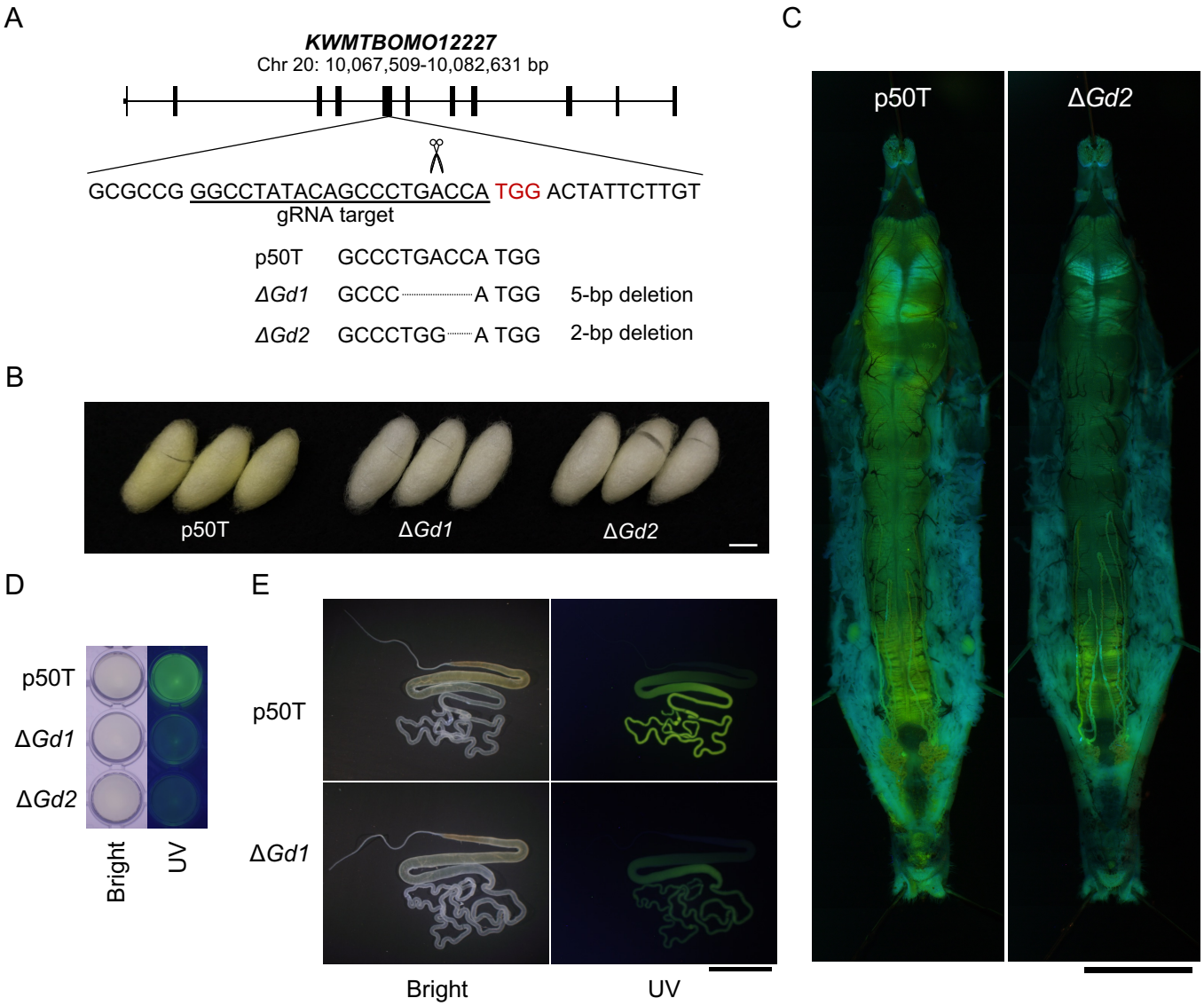


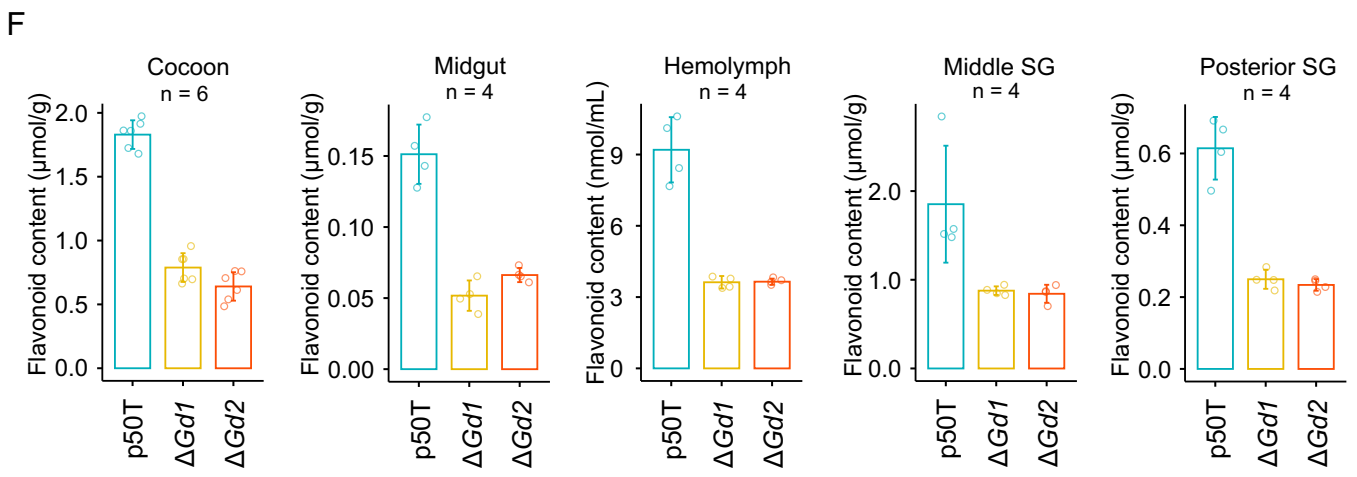


Fig 2. Reduction of flavonoid content in *KWMTBOMO12227*-knockout mutants.

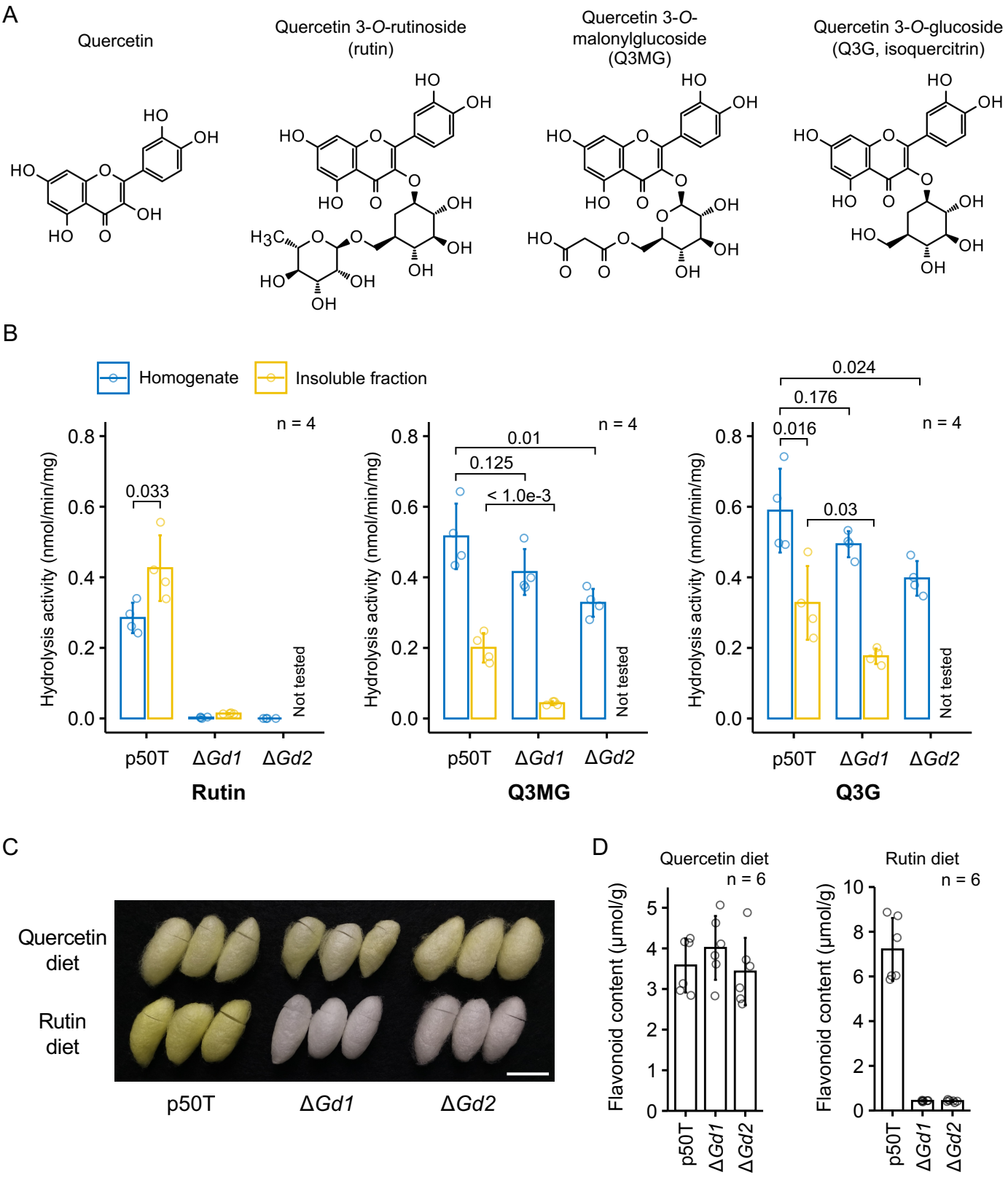


Fig 3. Hydrolytic activity of KWMTBOMO12227 on the three major quercetin glycosides in mulberry leaf.

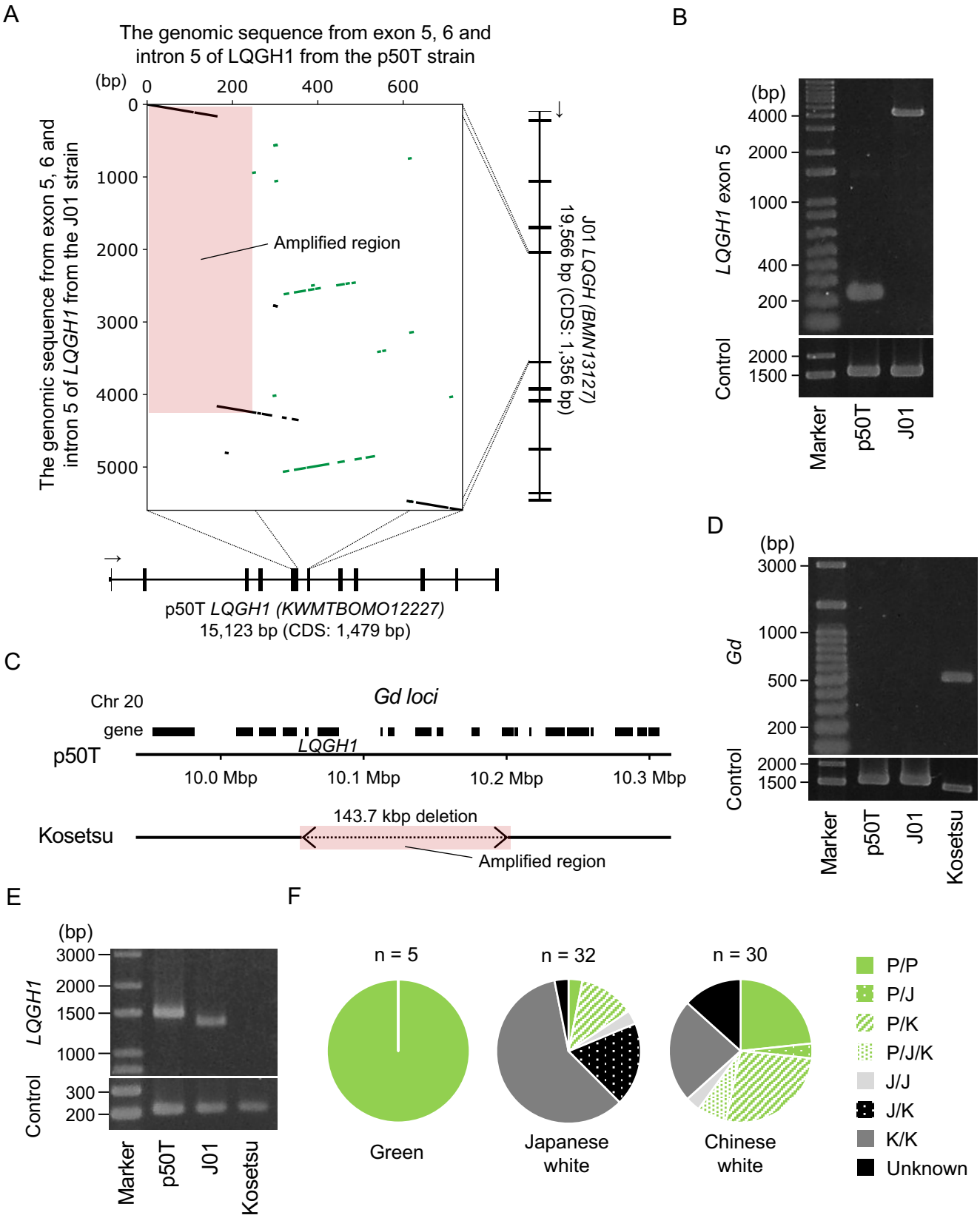


Fig 4. Conserved structural mutations of *LQGH1* in the domestic silkworm population.

S1 Fig. Photographs of representative cocoons of the wild silkworm, *Bombyx mandarina*.

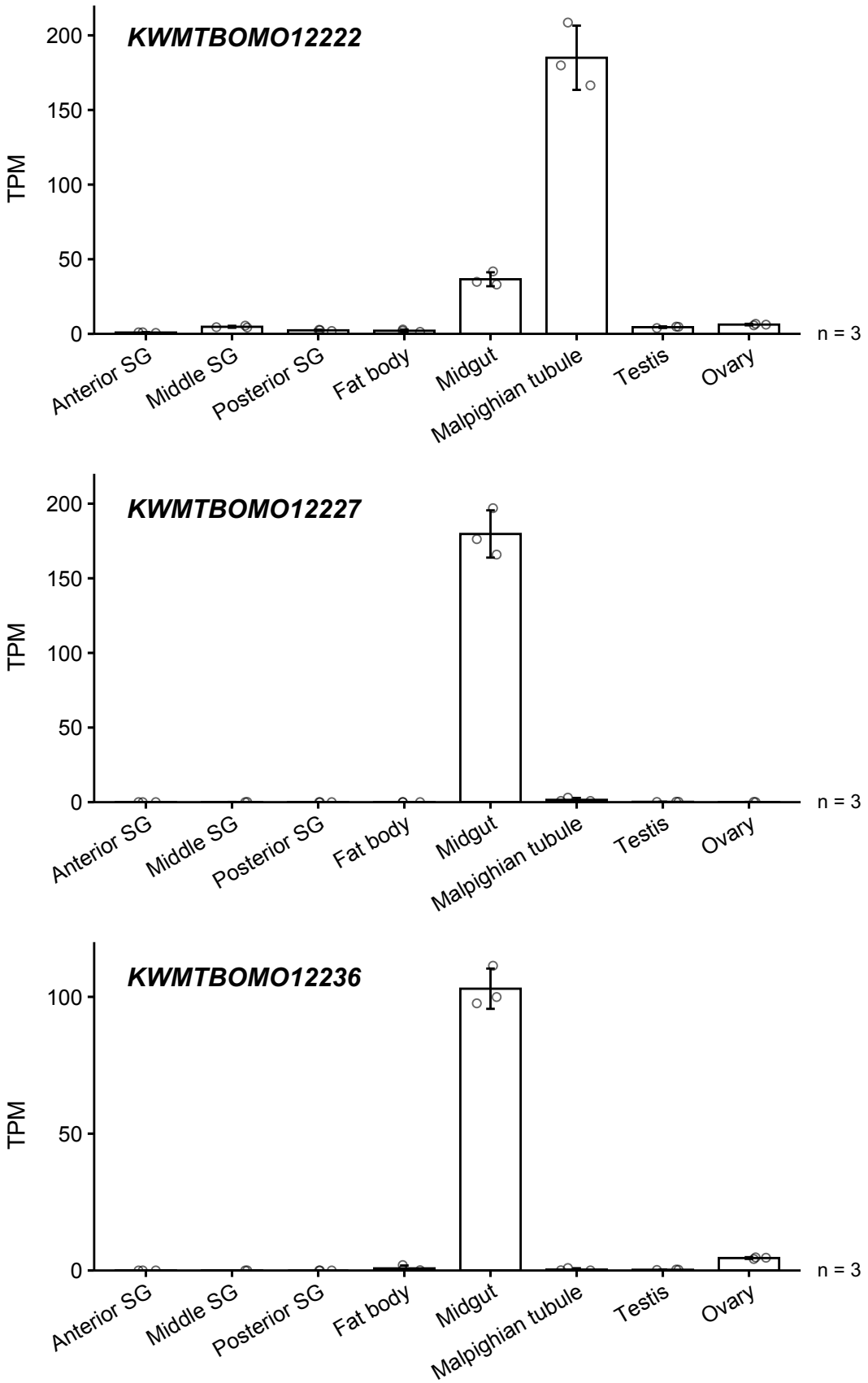


S2 Fig. Expression profile of the candidate genes within the *Gd* locus in third-day final instar larva of the p50T strain.

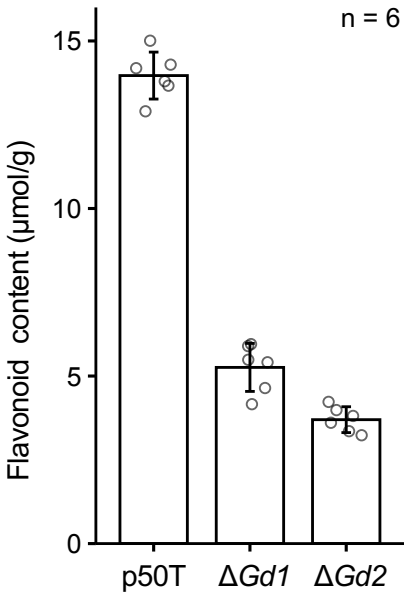


S3 Fig. Total flavonoid content in the cocoons of the p50T strain and the *KWMTBOMO12227*-knockout lineages reared on fresh mulberry leaves.

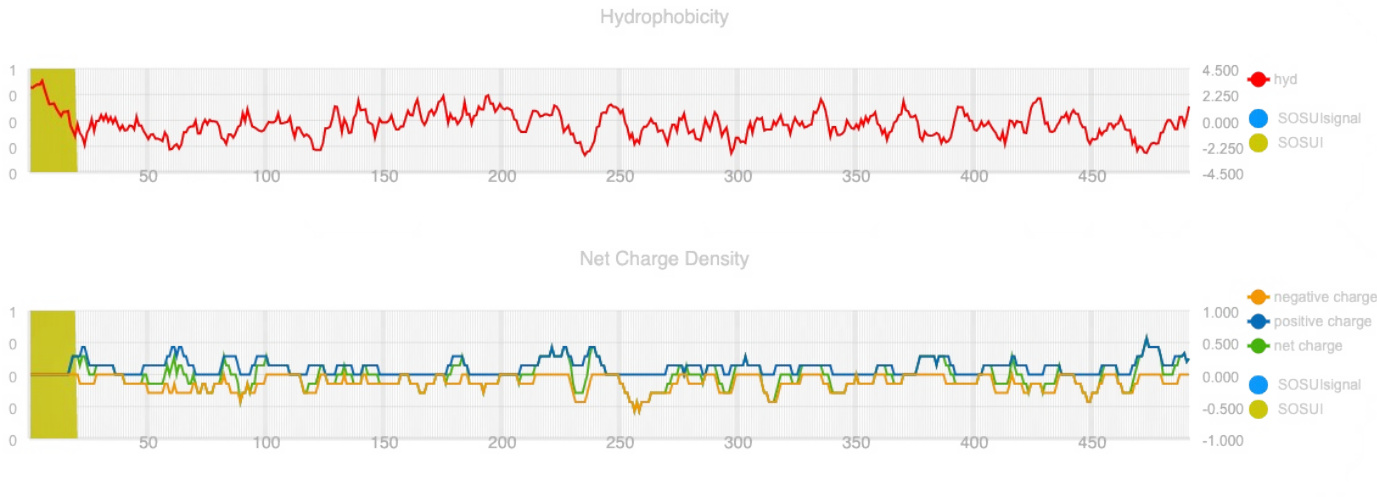


S4 Fig. Prediction of a transmembrane domain in the amino acid sequences of KWMTBOMO12227 by using the SOSUI tool.

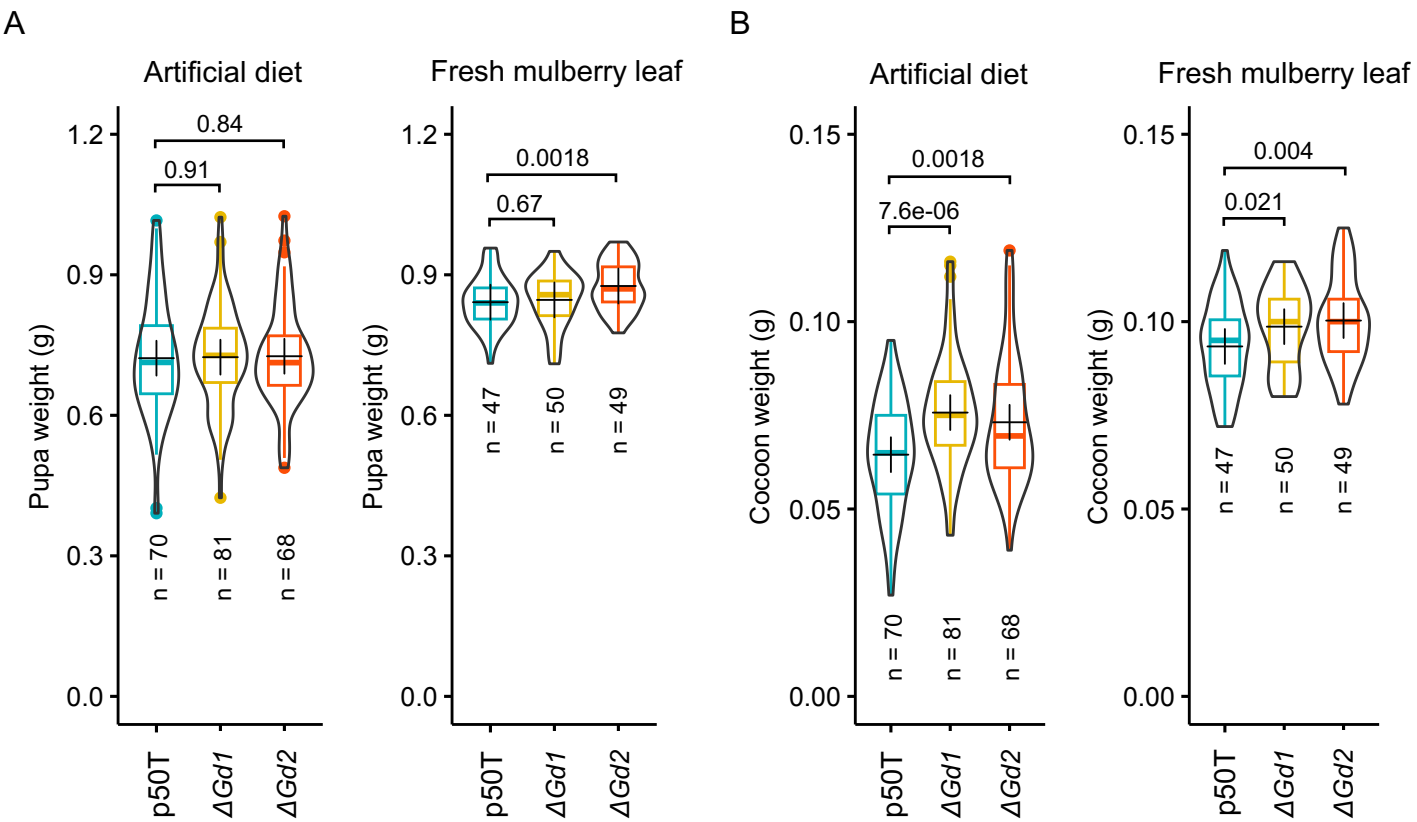


S5 Fig. Weight of pupa and cocoon of p50T and the knockout mutants of *LQGH1*.

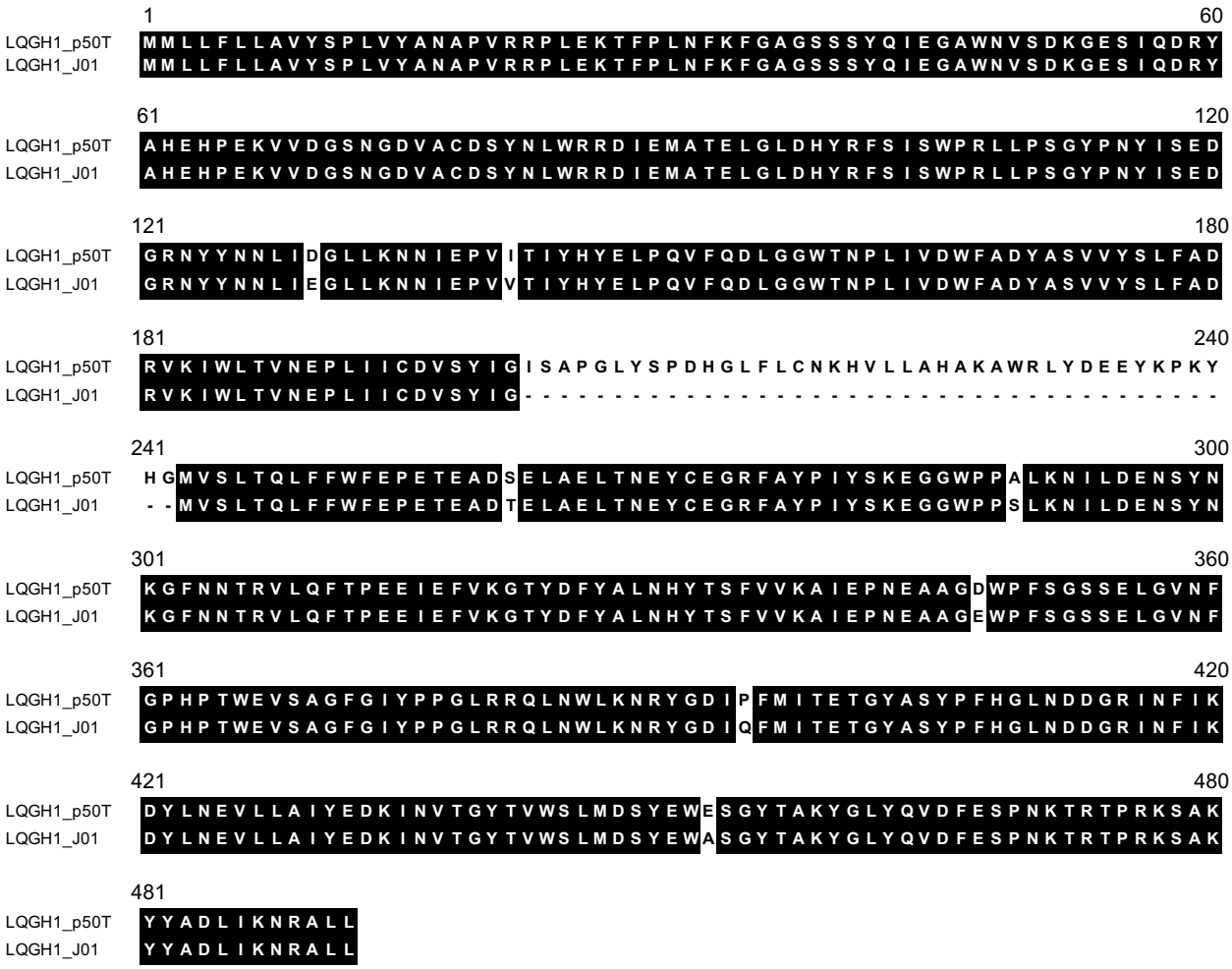


S6 Fig. Alignment of amino acid sequences of LQGH1 from the p50T and J01 strains.

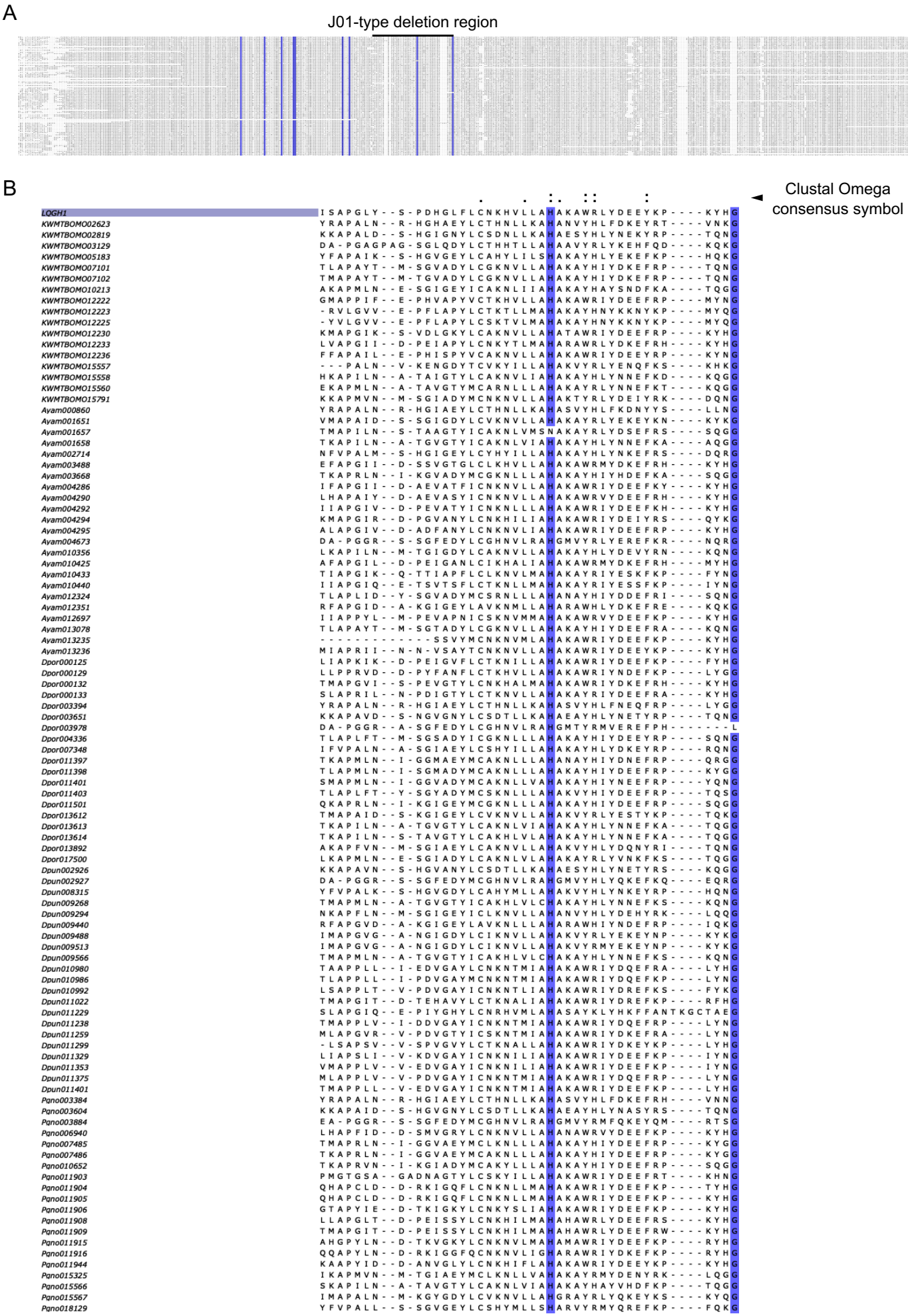


S7 Fig. Alignment of LQGH1-like proteins in Macroheterocera species.

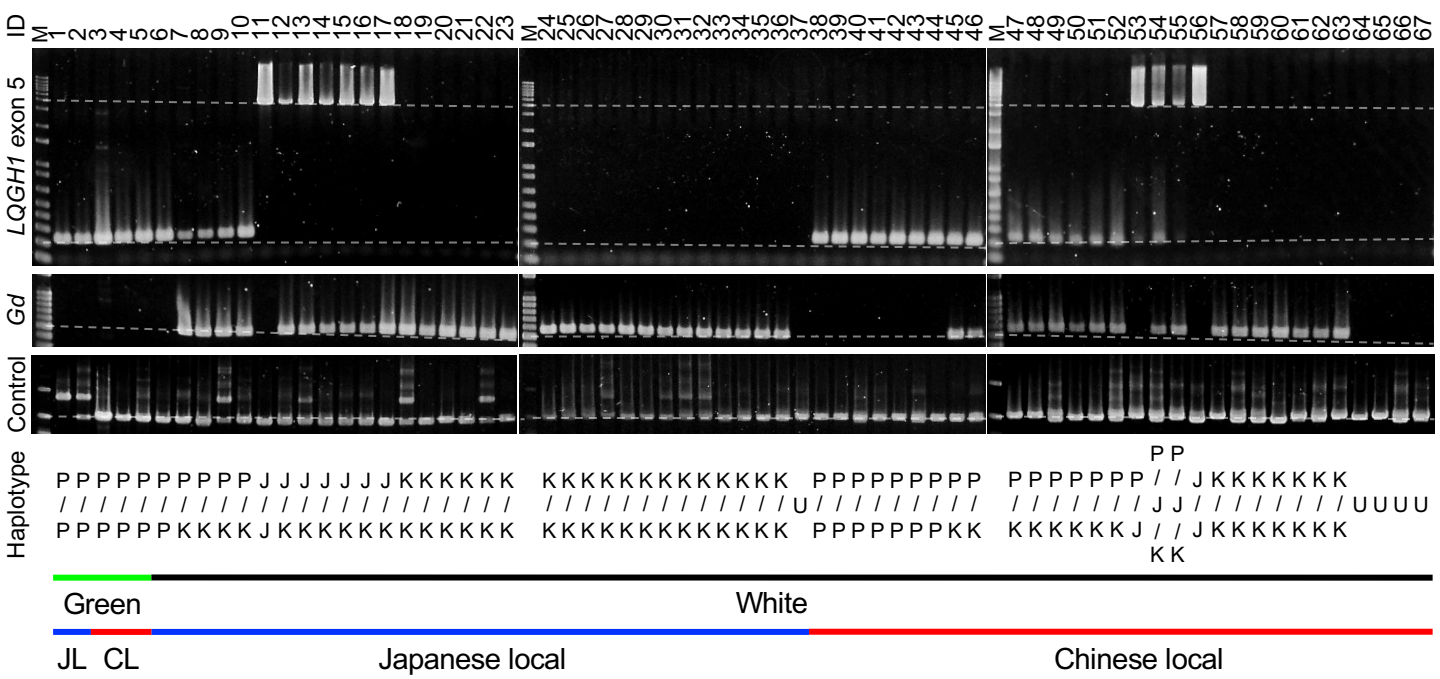


S8 Fig. Genotyping of the *Gd* locus of Japanese or Chinese local white-cocoon strains.

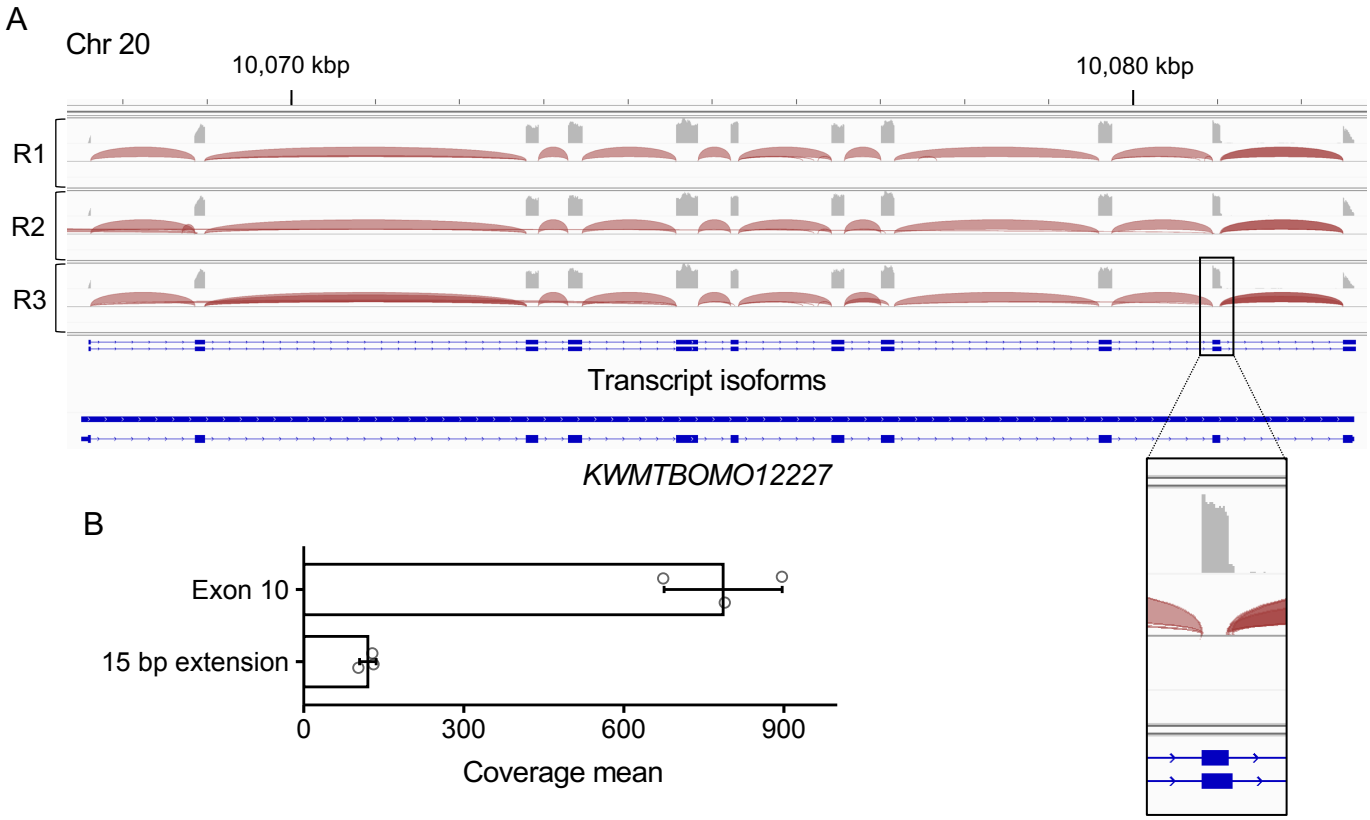


S9 Fig. RNA-seq read alignment to the genomic sequence of *KWMTBOMO12227* .

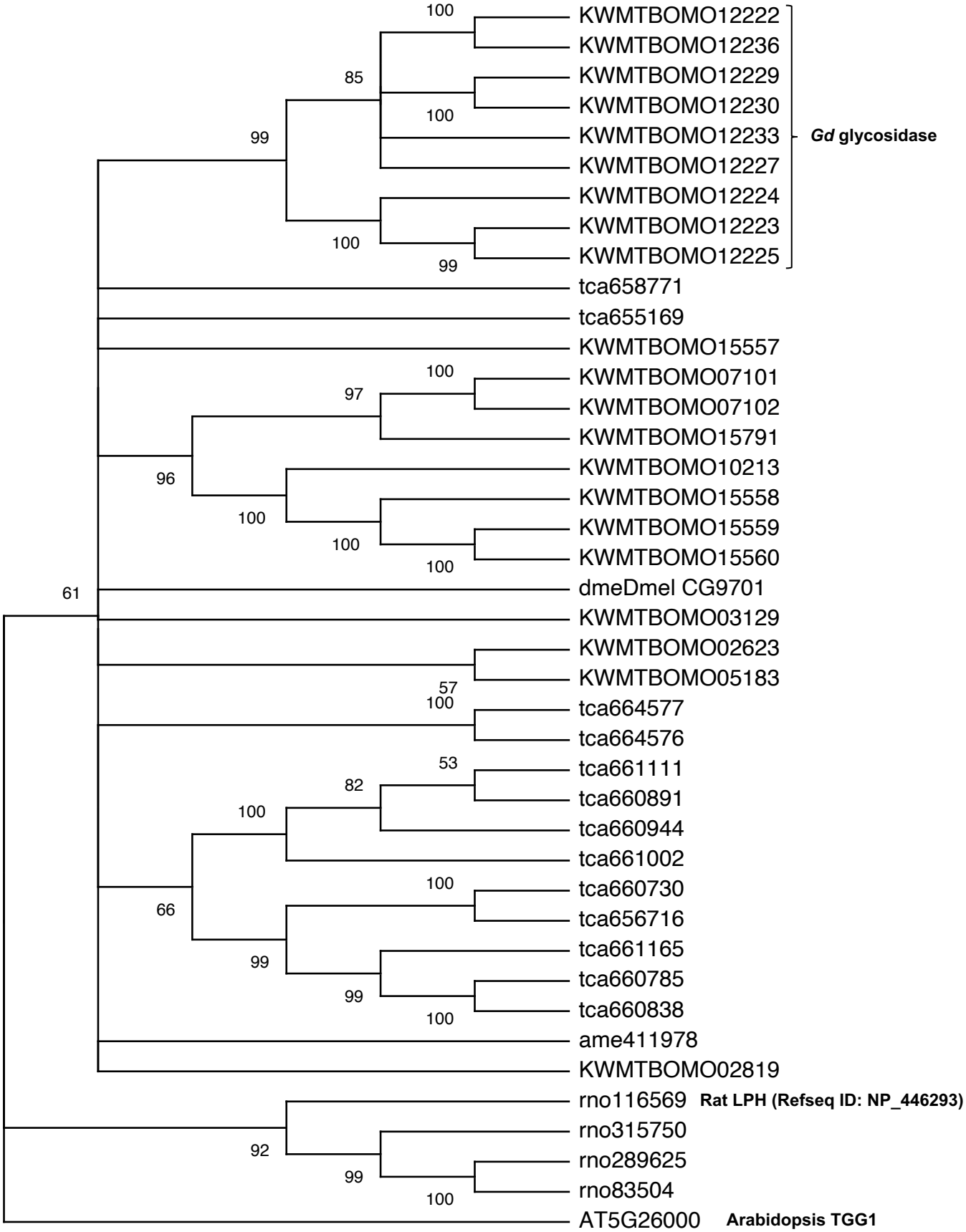


*Bombyx mori* (KWMTBOMO)
*Rattus norvegicus* (rno)
*Drosophila melanogaster* (dmeDmel)
*Tribolium castaneum* (tca)
*Apis mellifera* (ame)

S10 Fig. Phylogenetic tree of insect and rat proteins related to KWMTBOMO12227.

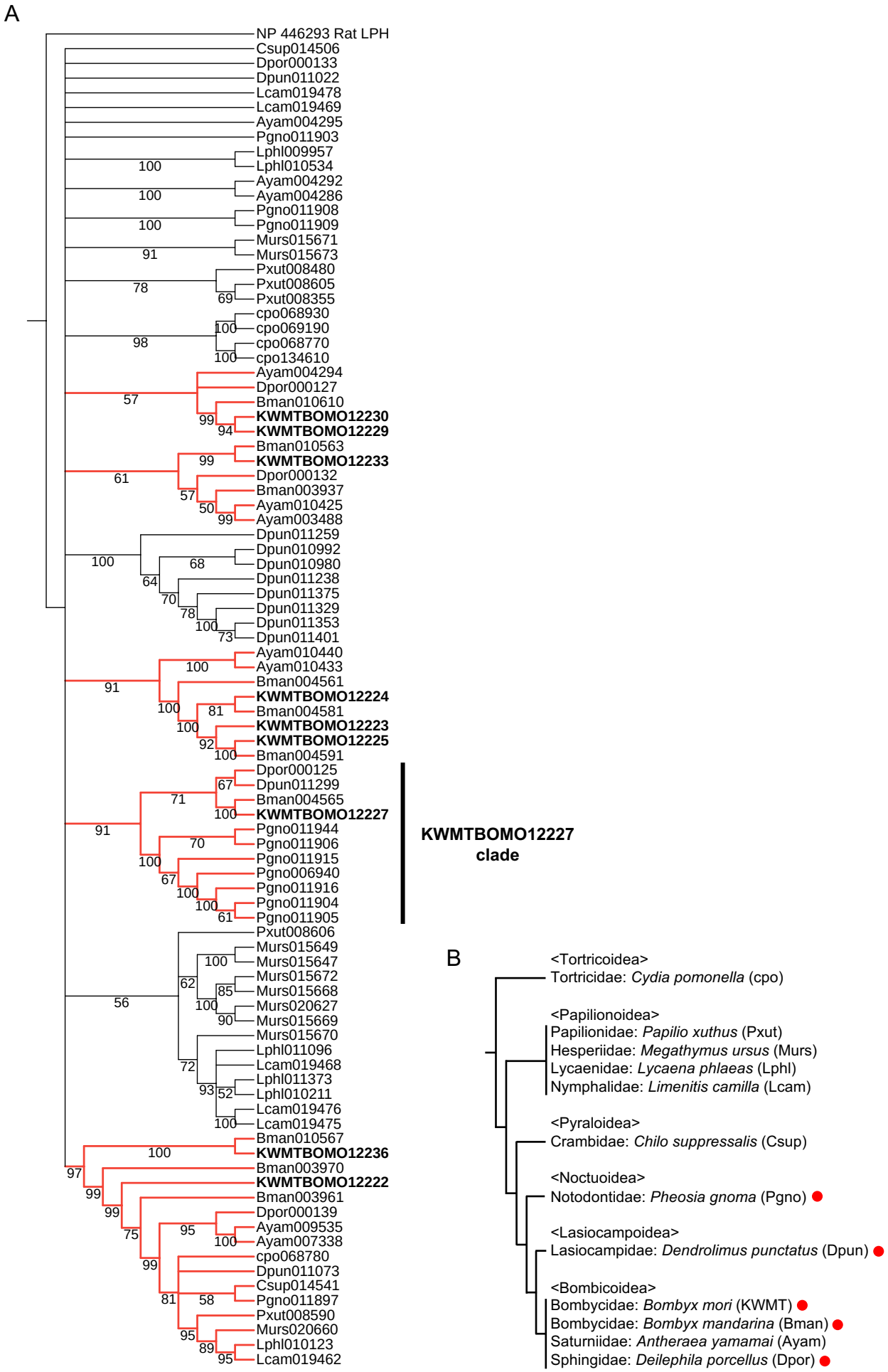


S11 Fig. Phylogenetic tree of *Gd* glycosidase orthologs in Lepidoptera.